



# **Powder flow and mixing in a continuous mixer operating in either transitory or steady-state regimes: Mesoscopic Markov chain models**

Chawki Ammarcha, Cendrine Gatumel, Jean-Louis Dirion, Michel Cabassud, V. Mizonov, Henri Berthiaux

## **► To cite this version:**

Chawki Ammarcha, Cendrine Gatumel, Jean-Louis Dirion, Michel Cabassud, V. Mizonov, et al.. Powder flow and mixing in a continuous mixer operating in either transitory or steady-state regimes: Mesoscopic Markov chain models. Powder Technology, 2019, 346, pp.116-136. 10.1016/j.powtec.2019.01.085 . hal-02013428

**HAL Id: hal-02013428**

**<https://imt-mines-albi.hal.science/hal-02013428>**

Submitted on 10 Apr 2019

**HAL** is a multi-disciplinary open access archive for the deposit and dissemination of scientific research documents, whether they are published or not. The documents may come from teaching and research institutions in France or abroad, or from public or private research centers.

L'archive ouverte pluridisciplinaire **HAL**, est destinée au dépôt et à la diffusion de documents scientifiques de niveau recherche, publiés ou non, émanant des établissements d'enseignement et de recherche français ou étrangers, des laboratoires publics ou privés.




## Open Archive Toulouse Archive Ouverte (OATAO)

OATAO is an open access repository that collects the work of Toulouse researchers and makes it freely available over the web where possible

This is an author's version published in: <http://oatao.univ-toulouse.fr/23675>

**Official URL:** <https://doi.org/10.1016/j.powtec.2019.01.085>

### **To cite this version:**

Ammarcha, Chawki and Gatumel, Cendrine and Dirion, Jean-Louis and Cabassud, Michel  and Mizonov, Vadim and Berthiaux, Henri *Powder flow and mixing in a continuous mixer operating in either transitory or steady-state regimes: Mesoscopic Markov chain models*. (2019) Powder Technology, 346. 116-136. ISSN 0032-5910

Any correspondence concerning this service should be sent  
to the repository administrator: [tech-oatao@listes-diff.inp-toulouse.fr](mailto:tech-oatao@listes-diff.inp-toulouse.fr)

# Powder flow and mixing in a continuous mixer operating in either transitory or steady-state regimes: Mesoscopic Markov chain models

Ammarcha C.<sup>a</sup>, Gatumel C.<sup>a</sup>, Dirion J.L.<sup>a</sup>, Cabassud M.<sup>b</sup>, Mizonov V.<sup>c</sup>, Berthiaux H.<sup>a,\*</sup>

<sup>a</sup> Université de Toulouse, IMT – Mines Albi-Carmaux, UMR CNRS 5302, Centre RAPSODEE, Campus Jarlard, F-81013 Albi Cedex 09, France

<sup>b</sup> Laboratoire de Génie Chimique, Université de Toulouse, CNRS, INPT, UPS, Toulouse, France

<sup>c</sup> Department of Applied Mathematics, ISPEU, Rabfakovskaya 34, 153003 Ivanovo, Russia

## ARTICLE INFO

### Keywords:

Powder mixing  
Markov chain  
Continuous mixing  
Transitory regime

## ABSTRACT

Continuous powder mixing is gaining interest in the industrial community concerned with more and more functional powder products. The understanding of powder flow and mixing/segregation of particles as well as their translation into models that can be used in process monitoring and control is a major issue. In the present work, we describe the development of different mesoscopic Markov chain models that are based on interconnected compartments or cells delimited in the mixing chamber. The general structure of the chain allows the derivation of either homogeneous or non-homogeneous markovian models, for which transition probabilities are state-dependent.

The models can be adapted to simulate variations of outflow rate, outlet mixture composition, hold-up weights and the distribution of these at the level of the compartments, during processing, including stationary and transitory phases. This is applied to a Gericke 500 GCM® continuous mixer for either pure powders or their mixtures, in the latter case through the consideration of a Markov chain for each component. The models are fed by independent experiments that allow for the determination of the probabilities and the rules governing their change with the processing step, in particular during the transitory regimes. Agreement is found between model calculation and experimental data for a wide range of configurations. The models can catch the variations of hold-up weights and internal or outlet flow rates at any rotational stirrer's speed during mixer start and steady state. They can reproduce the variations of the outflow rate, and therefore mixture composition, when dealing with a mixture of two components. This is also presented for two nominal compositions.

Conclusions are drawn in terms of process monitoring and control. It gives insights for process intensification, in particular for mixer design and the feeding configuration.

## 1. Introduction

Powder mixtures, or materials that once have been under the form of a powder mixture, are omnipresent in our everyday life. Metal alloys, cooking species, pharmaceutical pills or special concrete are current examples, and some can be made of up to twenty powder components depending on what the formulation stage has designed in terms of functionalities. Complexity of nowadays mixtures certainly lays in various factors, but can be wrapped by the idea that particles to mix are more and more of radically different rheological character, a statement that has been possible to make by the generalization of the FT-4 powder rheometer in both academia and industry over the past years. But while this growing demand for more technological mixtures, targeting specific properties at the consumer's scale, has been experienced during the last two decades, it has not been accompanied by a major

improvement from the part of the commercial mixing technologies themselves. Despite of the slow emergence of some more “chaotic” blenders, such as the Nautamixer® and the Turbula® mixer, the situation depicted by Bridgwater at the beginning of the present decade [11] still holds true: mixing equipment in the industry are still the basic tumbler, ribbon or plough blenders, most of the time driven in the batch mode.

Continuous mixers can be seen as a viable alternative to face the challenges of today's functional mixtures:

- The increase of ingredients, which is cumbersome to handle for batch mixers to what concerns the order of introduction of the powders, is just replaced by an increase of the number of Loss-In-Weight (LIW) feeders.
- Before entering the final continuous mixing step, ingredients can be premixed according to their rheological compatibilities or targeted functionalities. The premix can be performed either in continuous or batch, depending on the quantities involved.

\* Corresponding author.

E-mail address: [berthiau@mines-albi.fr](mailto:berthiau@mines-albi.fr) (H. Berthiaux).

- On-line analysis of the quality attributes of the products or intermediary has developed strongly over the past years and can be adapted to measure each of these functionalities in real-time.
- The operator-dependency, which is strong for batch processes, vanishes almost completely for continuous ones.
- Obviously, classical advantages hold true: reduced volume, simplified scale-up and process validation, reduced waste and energy, easier link with yet continuous operations.

A good example of the batch to continuous dilemma for powders can be found in the pharmaceutical industry and is worth referring to. Anyone that has ever been concerned with powder mixing knows that the pharma industry can serve as the industry of reference because it is the only one that integrates standards on mixture homogeneity in its own norms and rules. Regulatory agencies such as the FDA in the US or the ANSM in France pushed the sector to develop the so-called Process Analytical Technologies (PAT) at the beginning of the 2000's in order to ensure the quality of the products (see [36]). Pharmaceutical firms had to develop ways of controlling "critical quality attributes" on-line, and in particular blend uniformity. This motivated analytical equipment vendors to adapt their equipment to the pharma environment and stimulated industry-academia collaborations, that in turn left footprints in the scientific literature of that period (see for example [15,30,53]). Fifteen years later, and as pointed out by Roche et al. [40] as well as Ierapetritou et al. [22], the FDA officially recommended the shift from batch to continuous processes. At that time, big pharma companies, such as Pfizer, BMS and Sanofi had already began their own transformation on a number of production lines. Today, companies of less international impact, such as Servier or Pierre Fabre in France are joining the movement.

In parallel to this industrial evolution, the understanding of continuous powder processing in general and continuous mixing in particular from a chemical engineering standpoint has been the fact of very few research teams in the world and drew limited published works (see the paper by [34] on the situation at the time of their review). The following sub-areas of research on continuous powder mixers have been investigated:

- Definitions of mixture quality and mixer performance.

The definition of mixture's homogeneity requires first the determination of a key component of the mixture: it can be the active pharmaceutical ingredient, the bleaching agent, starch for icing sugar, etc. Homogeneity is then calculated (or estimated) by cutting the mixture into  $N$  portions (or considering  $n$  samples from the mixture) of size equal to that of the scale of scrutiny, to further derive the variance  $\sigma^2$  (or  $s^2$ ) of the compositions  $x_i$  in the key ingredient. If  $\mu$  (or  $x_m$ ) is the mean content in key component in the mixture (or in the sampling set):

$$\mu = \frac{1}{N} \sum_{i=1}^N x_i \quad \sigma^2 = \frac{1}{N} \sum_{i=1}^N (x_i - \mu)^2 \quad (1)$$

$$x_m = \frac{1}{n} \sum_{i=1}^n x_i \quad s^2 = \frac{1}{n} \sum_{i=1}^n (x_i - x_m)^2 \quad (2)$$

Usually, the coefficient of variation, which is the ratio between the standard deviation and the mean, is better considered. It actually serves as a standard for pharma blend release on the market, as far as its value lies below 6%.

This set of definitions is well adapted for batch mixing because it reflects the spatial distribution, and discrepancy in compositions, inside the equipment. But for continuous mixers, while the spatial distribution of the particles inside the mixer contributes to the building of a good mixture, it is not relevant to the definition of mixture homogeneity: only the outlet's mixture is of importance as it is the one that must pass quality controls. As a result, its variance calculation will be based

on the consideration of a set of  $N$  consecutive samples, a "window" of samples, taken at the outlet of the blender [18]. Therefore, Eqs. (1)–(2) are still holding true, but for a well-defined time period of production corresponding to that window of  $N$  samples.

Finally, and as pointed out by Weinekötter and Reh [51], a continuous mixer serves as a system able to reduce the spread in compositions between the inlet and the outlet of the equipment. Mixer performance is therefore evaluated by calculating the Variance Reduction Ratio (VRR), which is the ratio between the inlet variance and the outlet variance.

- Effects of operating variables at steady-state.

Most of the academic work done so far to what concerns continuous powder mixers concerns the effect of the operating variables on either the bulk particle flow or the mixture quality while the equipment is at steady-state. Marikh et al. [27] first investigated the effect of the rotational speed of the stirrer before publishing their work on the effect of the stirrer design on the hold-up weights and homogeneity of a commercial pharmaceutical mixture [29]. They emphasized the effect of the different flow regimes that can take place according to the choice of the operating variables. Effects of blade configuration, mass flow rates, and again stirrer's rotational speed, have been reported over the same period of time for pharmaceutical systems by Prof Muzzio's team in New Jersey (see [33,38,49]). The work of Kingston and Heindel [24] on the effect on the rotation mode (co-rotating, counter-rotating, down or up-pumping) in a double-screw continuous mixer is also worth noting.

- Flow models and mixing models.

Modelling both the bulk particle flow and the blending of particles of different nature is undoubtedly the key in the understanding of continuous powder mixers. Kehlenbeck and Sommer [23] developed a two-dispersion coefficient (one for each component) model for a Gericke GCM 500 mixer. They identified the coefficients from the mathematical fitting of the results, which makes this model semi-empirical. Some years later, a Distinct Element Model (DEM) was being published by Sarkar and Wasgren [42] for spherical identical particles. This allowed the authors to derive local dispersion coefficients and define flow regimes according to a Froude number in a section of the mixer concerned with approximately  $10^4$  particles. Although this is quite far from the real number of particles involved in an industrial mixer, for which wall effects cannot be forgotten, this study caught some tendencies revealed earlier by Positron techniques [25] and shown that DEM can be employed as a building block for macroscopic models.

The need for a more global model, possibly able to include more microscopic thoughts, has then been the rule in modelling powder mixers. Sen et al. [43] and then Sen and Ramachandran [44] developed a Population Balance Model (PBM) to simulate data of Residence Time Distributions (RTD) obtained in Gericke GCM 250. The model formulation, although continuous in time and space, needs discretization and is finally close to a compartment model. The periodic section model developed by Gao et al. [21] can be classified into this same category. These authors compared the model results with RTD data obtained numerically and found good consistency. They emphasized the idea that their model do not include particle diversity and that segregation is still a challenge to account for in modelling. Another class of model uses the Markov chain approach and can be viewed as a generalization of compartment models. As we will apply this modelling tool in the present work, the lector may refer to the specific section dedicated to it.

- Transitory operation and first process control strategies.

While a continuous mixer is aimed to operate at steady-state, transitory phases are taking place currently during normal production. First,

the equipment must start, which means that the hold-up weight will rise during a certain period of time before reaching a steady value, according to the operational conditions. Then, LIW feeders must be fed during processing which drives to strong perturbations because the volumetric mode of dosage is less accurate [10]. Finally, mixers must be emptied, again conducting to a transitory period for which process outcomes are decreasing and mixture quality is impacted. In previous works [1,2], we investigated the influence on hold-up weight and out-flow rates (still on the GCM 500) of various transitory phases, namely: emptying, starting and step-changes on the rotational speed  $N$  of the stirrer. We focused only on the bulk particle flow (no mixture) and derived empirical correlations through the frame of a single cell Markov chain model. Later on [3], we developed a system for on-line image analysis of simple mixtures, able to capture all the particles flowing out of the equipment and calculate mixture homogeneity in real-time. The influences of the scale of scrutiny, as well as that of  $N$ , on the quality of the mixtures were demonstrated. But the main outcome was that it was possible to evidence the extent of segregation in the mixer, as the mixtures produced during the starting phase were richer in coarse particles (fines were accumulating in the equipment). This impacted clearly the quality of the mixtures when considering increasing step-perturbations on  $N$ , contrarily to negative steps.

The understanding and modelling of the transitory regime for a definite continuous mixer is also a prerequisite to monitoring and control of the operation, which can be viewed as the ultimate goal in the industrial implementation of such technologies. Published works by Ramachandran et al. [39], as well as Singh et al. [45] were concerned mostly by the compaction process, but gave general thoughts on the possible control strategies. From our side, we communicated on our first results on the regulation of the GCM 500 in the 2013 AIChE's annual meeting [54].

To sum up this small specific literature survey, it can be said first that it is far from being abundant, mainly the fact of 2–3 research teams in the world. One of the major ideas is that there is a fundamental need to explore what is going on inside continuous mixers and account for particle segregation. As we experienced ourselves, it seems that segregation “dictates” the bulk particle flow inside the mixer, and cannot be considered as an epiphenomenon. The parallel development of systemic/compartiment models, that may in a second approach include DEM, to capture the process dynamics and be readily employed for process monitoring is also at stakes.

In the present work, we aim at developing and testing a mesoscopic model that accounts for the internal hold-ups and flow distributions inside the GCM 500 mixer. The objective is to derive a tool that could simulate and predict the behavior of the mixer in terms of outflow rates and mixture quality during both steady-state and transitory phases. For this, we will first focus on determining the distribution of the powder mass inside the mixer. This will then allow the determination of internal transition probabilities to be integrated in a mesoscopic Markov chain model. Model testing and validation will be presented in terms of out-flow rate and mixture quality evolution during steady-state operation, as well as starting up and strong perturbations on the rotational speed of the stirrer.

## 2. Experimental set-up and methods

### 2.1. Mixer

The mixing vessel studied in this work is the Gericke GCM 500 continuous mixer, equipped with two LIW feeders able to deliver a mass flow rate up to  $50 \text{ kg h}^{-1}$  each (see Fig. 1a). The hemicylindrical vessel is 50 cm long and 20 cm diameter. The mixing action is performed by a system of 10 blades mounted on a frame, whose axis is occupied by a screw-type shaft (Fig. 1b). The blades are ensuring a radial dispersion of the particles, while the screw is responsible for the axial movement of the bulk towards the outlet. Overall inlet

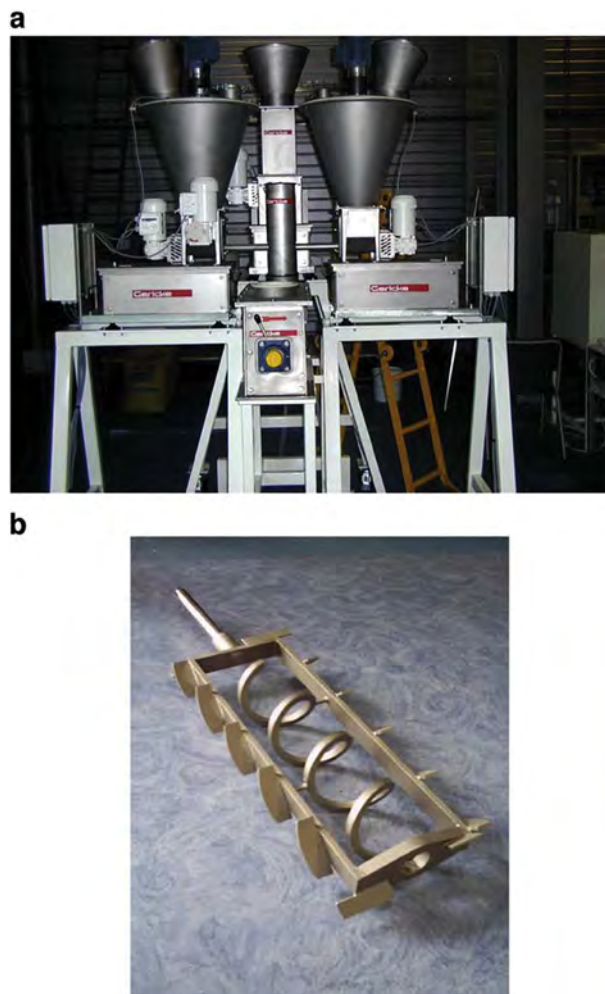


**Fig. 1.** Gericke GCM 500 facility showing the inlet chute, the mixing chamber, the LIW feeders (a); Stirring device used in this work (b).

mass flow rate  $Q_{in}$  as well as rotational stirrer speed  $N$ , are defining the hold-up weight in the equipment. A too small ratio  $Q_{in}/N$  will drive to a nearly-complete emptying of the mixing chamber, while a too high ratio may lead to overflow and mixer shutdown. The range of rotational speed values is 10 to 50 Hz for a global mass flow rate that lies between 10 and  $100 \text{ kg h}^{-1}$ . In the present work, the inflow rate will be kept constant at  $40 \text{ kg h}^{-1}$ .

### 2.2. Particulate systems

Our goal is to gather the maximum information available so as to model the mixing process itself, letting the particulate system considered as secondary. As in previous studies, we have chosen coarse and/or fine couscous, depending on whether a “pure” product or a mixture of both is investigated. This system has the following advantages:

- Shape and density of the particles are identical, which leaves the particle size as the sole difference, so as to give a clearer interpretation of the results.
- These products have experienced a cooking process, which confer them a certain time-stability.
- Products are cheap and easy to get hold of, which is important when high amounts of powders are to be handled.
- Mixtures can be analyzed easily through the image analysis method developed in earlier works.
- Mixtures can be separated by sieving and products can be re-used, as there is no overlap of the particle size distributions.



**Table 1**

Main physical characteristics of the powders used. Particle size has been determined by sieving, true density by He pycnometer and apparent bulk densities by Erweka® "tap-tap" volumenometer. Carr and Hausner ratios are deduced from bulk densities.

Considered property	Coarse couscous	Fine couscous
$d_{10}$ ( $\mu\text{m}$ )	1375	680
$d_{50}$ ( $\mu\text{m}$ )	1700	860
$d_{90}$ ( $\mu\text{m}$ )	1970	980
$(d_{90} - d_{10})/2 \cdot d_{50}$	0.175	0.170
True density $\rho$ ( $\text{kg.m}^{-3}$ )	1452	1442
Aerated apparent density $\rho_a$ ( $\text{g.m}^{-3}$ )	762	759
Tapped apparent density $\rho_t$ ( $\text{kg.m}^{-3}$ )	779	787
Carr index: $100 \cdot (\rho_t - \rho_a)/\rho_t$	2.22	3.60
Hausner ratio: $\rho_t/\rho_a$	1.02	1.04

Table 1 gives the major physical characteristics of the products, in terms on both individual and collective properties. Both products are free-flowing as indicated by the Carr index. Fine couscous particles have been previously colored in black thanks to a process of iodine adsorption first described in Aoun-Habbache et al. [4]. This allowed a color contrast with the (white-yellow) coarse particles that could be detected by the image analysis system.

### 2.3. Determination of internal masses and flows

As stated, we need to access to the spatial-distribution and time-evolution of the hold-up weights and flow rates along the axis of the mixer, so as to implement these in a compartment-type markovian model. If we look at the blade configuration in the frame, it can be seen that opposite blades can be grouped two-by-two so as to define five compartments or cells, each comprised of two opposite blades. These cells are of equal volume.

Let  $M_i(t)$  be the powder mass in cell  $i$  at time  $t$ ,  $M_6(t)$  being the cumulative mass measured at the outlet of the equipment.  $M_i(t)$  has been measured experimentally by operating the mixer for the time  $t$ , stop it and then withdraw the whole powder mass corresponding to each cell by suction, beginning by cell  $n^\circ 5$ . This operation has been repeated for up to 17 times in the time interval 0–150 s. Let  $\Delta t$  be a time interval (in the present work  $\Delta t$  will be chosen as  $\Delta t = 0.1$  s). The net flowrate  $Q_{out,i}$  leaving cell  $n^\circ i$  between  $t$  and  $t + \Delta t$  reads:

$$Q_{out,i} = \frac{\sum_{j=i+1}^6 [M_j(t + \Delta t) - M_j(t)]}{\Delta t} \quad (3)$$

Therefore, internal flowrates between cells can be calculated by letting  $\Delta t$  be small enough to gain precision. In addition, if no back-mixing takes place in the mixer, the mean residence time in cell  $i$  can be derived as follows:

$$\tau_i(t) = \frac{M_i(t)}{Q_{out,i}(t)} \quad (4)$$

This procedure has been run for coarse couscous alone in the determination of bulk flow characteristics, as well as for each product (coarse and fine couscous) in the determination of mixture flow characteristics.

### 2.4. Mixture composition analysis

Part of the presented work will deal with mixtures of fine and coarse couscous. The analysis of these will be performed on-line by an image analysis ring that has been fully presented in Ammarcha et al. [3]. A belt conveyor is placed at the mixer's outlet so as to form a single layer of particles by adjusting its speed to the inflow rate considered. A CCD linear camera placed perpendicularly to the belt captures all the particles passing under the camera and a specific routine created on Labview® allows the analysis of the images. Data treatment is performed through threshold procedures in order to detect fine couscous particles (white) from coarse couscous particles (black) and the conveyor belt (green).

An image, which is the finest scale of scrutiny of the mixture that can be envisioned for our system, is defined by the accumulation of 200 consecutive single-pixel lines. Samples can be built by the grouping of various consecutive images, therefore defining various possible sample masses. In the present work, we will consider the grouping of 21 consecutive images that correspond to a sample mass of 17.8 g of powder mixture. Results for two mixture compositions will be presented in the last section of this paper, namely a 50–50% by weight mixture and a 12.5–87.5% mixture of coarse and fine couscous respectively.

## 3. Mesoscopic Markov chain models developed

### 3.1. Some generalities

A Markov chain is a mathematical tool that has been employed to model countless systems in any field of science, such as the recognition of words in handwritten letters [14], direct marketing [35] or the prevision of significant weather events [41] to name a few.

In powder processes, it has been considered for several operations and equipment:

- Grinding: Wei et al. [52], Auer [5], Berthiaux [8], Catak et al. [12]
- Filtration and sedimentation: Tory and Pickard [48], Nassar et al. [32]
- Classification: Berthiaux and Dodds [7]
- Agglomeration: Catak et al. [13]
- Fluidized beds: Fan and Chang [19], Dehling et al. [16], Zhuang et al. [55]
- Rotating drums: Fan and Shin [20], Tjakra et al. [47]
- Mixing: Wang and Fan [50], Aoun-Habbache et al. [4], Ponomarev et al. [37], Legoix et al. [26], Balagurov et al. [6]

For more insights on the applications of Markov chains in particulate systems engineering, the reader can refer to the review paper by Berthiaux and Mizonov [9].

A Markov chain model aims at describing a systems' dynamics. First, this system must be decomposed into a finite number of interconnected cells, also called "states". The intensity of these connections, are quantified as transition probabilities between the states. Most of the time, the cells are corresponding to a distribution of the physical space that may advisably be based on physical thoughts or visual

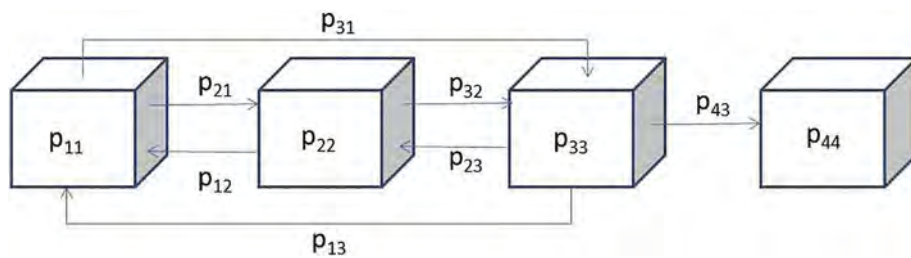


Fig. 2. Example of Markov chain.

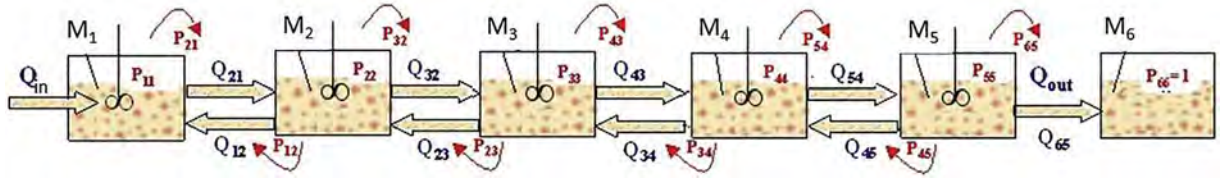


Fig. 3. General structure of the mesoscopic Markov chain representing the flow in the continuous mixer.

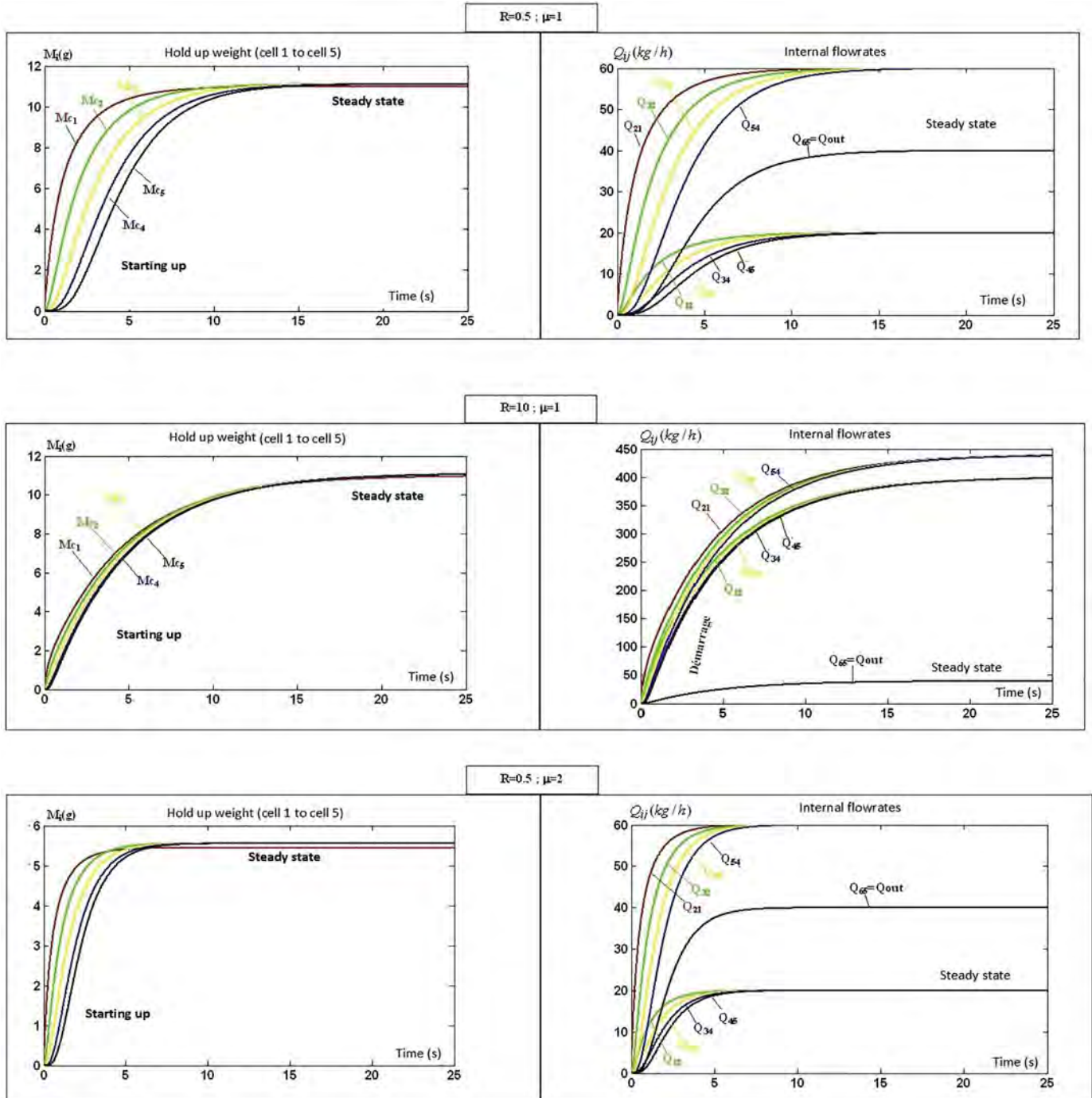


Fig. 4. Simulation of the evolution of the internal hold-ups and flowrates during the starting of a continuous mixer showing the influence of the recirculation ratio  $R$ .  $Q_{in} = 40 \text{ kg h}^{-1}$ ;  $\mu_i = 1 \text{ s}^{-1}$ .

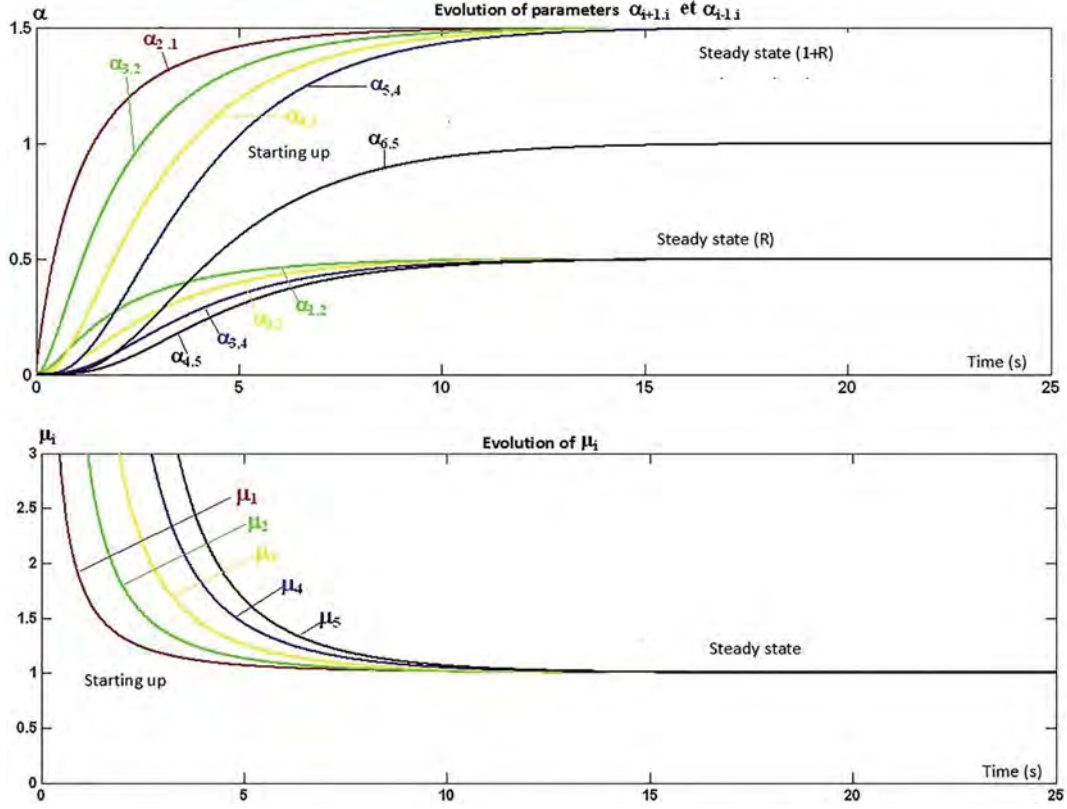


Fig. 5. Simulation of the changes in  $\alpha_{ij}(k)$  and  $\mu_i(k)$  during the transitory phase leading to their steady values.

observations. In addition, transition probabilities are usually relative mass flows between cells that may adjust to mass balances.

Consider the simple case depicted in Fig. 2 that may represent the flow of powders in a certain equipment. It consists of four states, one of them being an absorbing state, which means that nothing can flow out of it. An absorbing state can therefore represent the outlet of a process. Let us observe the system after  $n$  transitions (or after any time relative to a fix time interval) and be  $S(n)$  the state vector that represents the repartition of the powder in the four states  $S_i(n)$  after those  $n$  transitions ( $S(0)$  is the initial configuration):

$$S(n) = \begin{bmatrix} S_1(n) \\ S_2(n) \\ S_3(n) \\ S_4(n) \end{bmatrix} \quad (5)$$

Let  $p_{ij}(n)$  the transition probability, or the relative amount of powder transiting from cell  $j$  to cell  $i$  during the  $n$ th transition, and  $P(n)$  the transition matrix that gathers all the  $p_{ij}(n)$  values:

$$P(n) = \begin{bmatrix} p_{11}(n) & \cdots & p_{14}(n) \\ \vdots & \ddots & \vdots \\ p_{41}(n) & \cdots & p_{44}(n) \end{bmatrix} \quad (6)$$

In the present case:

$$p_{41}(n) = p_{31}(n) = p_{42}(n) = p_{13}(n) = p_{14}(n) = p_{24}(n) = p_{34}(n) = 0 \text{ and } p_{44}(n) = 1$$

If  $S(n)$  and  $P(n)$  are known,  $S(n+1)$  can be readily calculated by the recurring formula:

$$S(n+1) = P(n) S(n) \quad (7)$$

A Markov chain is said “homogeneous” when the transition probabilities are not varying with time or with the state of the system. In

this case Eq. (7) can be easily changed into:

$$S(n+1) = P^n S(0) \quad (8)$$

If  $P$  is not constant, the chain is considered “non-homogeneous”, subcases being: linear chain if  $P$  depends only on  $n$ ; non-linear chain if  $P$  depends both on  $n$  and  $S(n)$ . Transition probabilities can change with time or with the state reached by the system in many cases involving powders, as these can be compacted during the mixing process or experience variation in the kinetics of grinding for a size reduction process.

### 3.2. General structure of the markovian models developed

To account for the horizontal configuration of the mixer and of the powder flow inside the vessel with the possibility of back-mixing, a general Markov chain that consists of  $n-1$  cells allowing flows only between contiguous cells can be envisioned (Fig. 3). As mentioned previously, the  $n$ th state is absorbing and figures out the outlet of the blender. The inlet is represented by an arrow to which is attached the inlet flowrate  $Q_{in}$ . Let  $M_i(k)$  the powder mass in cell  $i$  and let  $Q_{ij}(k)$  be the flow rate from cell  $j$  to cell  $i$ , after the  $k$ th transition. In the model, only flowrates between contiguous cells are allowed. The model's structure lay between that of a full macroscopic black box model and that of a DEM model at the scale of a particle. It can be thought as a “mesoscopic model”.

If  $p_{ij}(k)$  is the transition probability for powders flowing from cell  $j$  to cell  $i$ , and  $\Delta F_1(k)$  the powder mass introduced (at the inlet, cell 1) in the mixer, the Markov chain can be established by the following rule:

$$M(k+1) = P(k)[M(k) + \Delta F_1(k)]$$



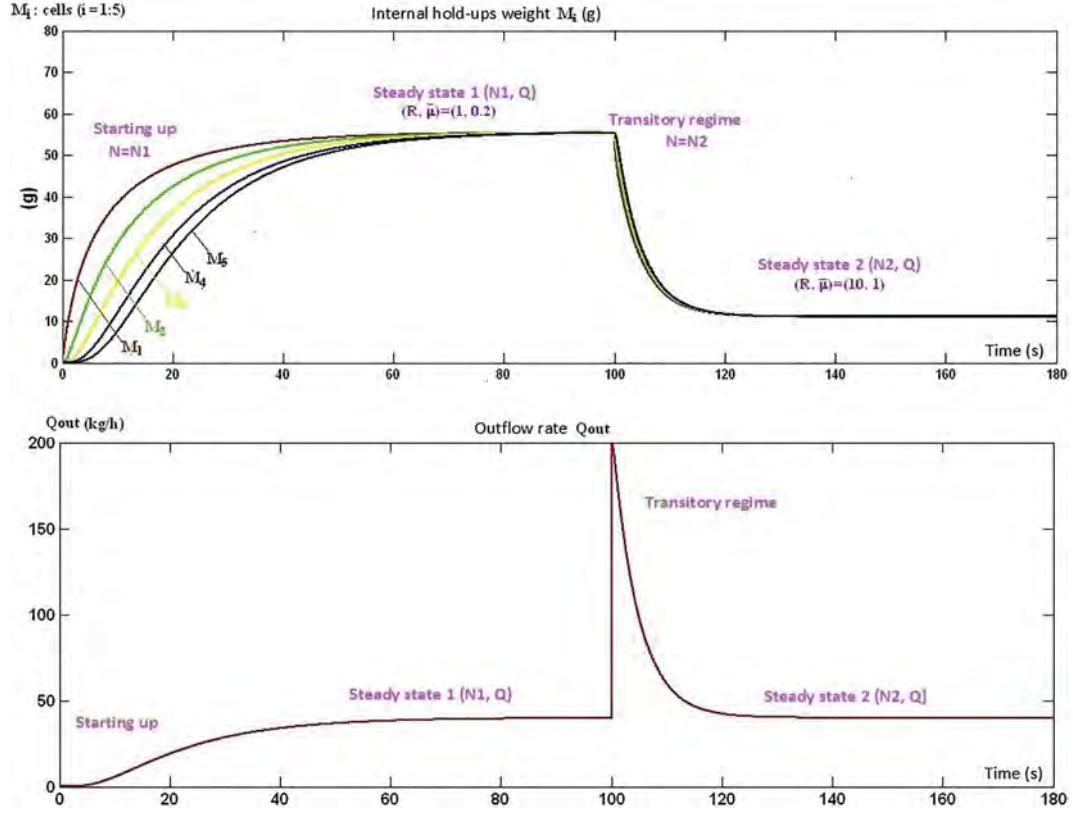


Fig. 6. Simulation of an instantaneous change of pair  $(R, \bar{\mu}_i)$  from  $(1, 0.2)$  to  $(10, 1)$  in terms of internal hold-ups and outflow rate.  $\Delta t = 0.005$  s,  $Q = 40$  kg h<sup>-1</sup>.

$$\begin{bmatrix} M_1(k+1) \\ M_2(k+1) \\ \vdots \\ M_{n-1}(k+1) \\ M_n(k+1) \end{bmatrix} = \begin{bmatrix} p_{11}(k) & p_{12}(k) & 0 & \dots & 0 \\ p_{21}(k) & p_{22}(k) & p_{23}(k) & \vdots & 0 \\ 0 & p_{32}(k) & p_{33}(k) & p_{n-2,n-1}(k) & \vdots \\ \vdots & 0 & p_{33}(k) & p_{n-1,n-1}(k) & \vdots \\ 0 & \dots & \dots & p_{n,n-1}(k) & p_{nn}(k) \end{bmatrix} \times \begin{bmatrix} M_1(k) + \Delta F_1(k) \\ M_2(k) \\ \vdots \\ M_{n-1}(k) \\ M_n(k) \end{bmatrix}$$

The above set of notations allows for the possibility of feeding the equipment in cells other than cell 1, or distributing the feeding alongside the mixer. If  $\Delta t$  is the time interval through which the system is observed, assuming the inlet flow rate does not change with time, we also have:

$$\Delta F_1(k) = Q_{in} \Delta t \quad (10)$$

Let  $\alpha_{ij}(k)$  the ratio between the flowrates  $Q_{ij}(k)$  and  $Q_{in}$ . We basically have:

$$Q_{i-1,i}(k) = \alpha_{i-1,i}(k) Q_{in} \text{ and } Q_{i+1,i}(k) = \alpha_{i+1,i}(k) Q_{in} \quad (11)$$

Let us consider cell 1. The probability  $p_{21}(k)$  for a particle to transit from cell 1 to cell 2 between the  $k^{\text{th}}$  and the  $k+1$ th state is the probability  $(1 - p_{11}(k))$  to leave state 1 during this transition. The corresponding mass leaving state 1 is therefore the product of  $(1 - p_{11}(k))$  by the mass present in state 1 after  $k$  transitions, which is  $M_1(k) + \Delta F_1(k)$ . As this mass can only arrive in state 2 and is attached to the flowrate  $Q_{21}(k)$ , we have the following equation:

$$[1 - p_{11}(k)][M_1(k) + \Delta F_1(k)] = Q_{21}(k) \Delta t \quad (12)$$

Replacing  $Q_{21}(k)$  by Eq. (11) through Eq. (12) gives:

$$p_{11}(k) = 1 - \alpha_{21}(k) \mu_1(k) \Delta t \quad p_{21}(k) = \alpha_{21}(k) \mu_1(k) \Delta t \quad (13)$$

Where:

$$\mu_1(k) = \frac{Q_{in}}{M_1(k) + \Delta F_1(k)} \quad (14)$$

A similar reasoning for the other cells drives to the following set of equations:

$$p_{ii}(k) = 1 - [\alpha_{i-1,i}(k) + \alpha_{i+1,i}(k)] \mu_i(k) \Delta t$$

$$p_{i+1,i}(k) = \alpha_{i+1,i}(k) \mu_i(k) \Delta t \quad (15)$$

$$p_{i-1,i}(k) = \alpha_{i-1,i}(k) \mu_i(k) \Delta t$$

where:

$$\mu_i(k) = \frac{Q_{in}}{M_i(k)} \quad (16)$$

Eqs. (15) and (16) allow the construction of the transition matrix  $P(k)$  and the full description of the dynamics in transitory regime, if the initial state is known (usually empty cells). Eq. (16) also shows that transition probabilities not only depend on  $k$  (or time), but also on the previous state of the system ( $M(k)$ ), which makes the general model non-homogeneous and non-linear.

When the mixer is at steady-state, all the back-mixing coefficients  $\alpha_{i-1,i}$  are equals to a single value  $R$ , which may be dependent on stirrer's design and rotational speed. The coefficients  $\mu_i$  are also of constant value, equal to  $\bar{\mu}_i$ , and can be seen as characteristic frequencies or inverse of geometric residence times, each relative to cell  $i$ .

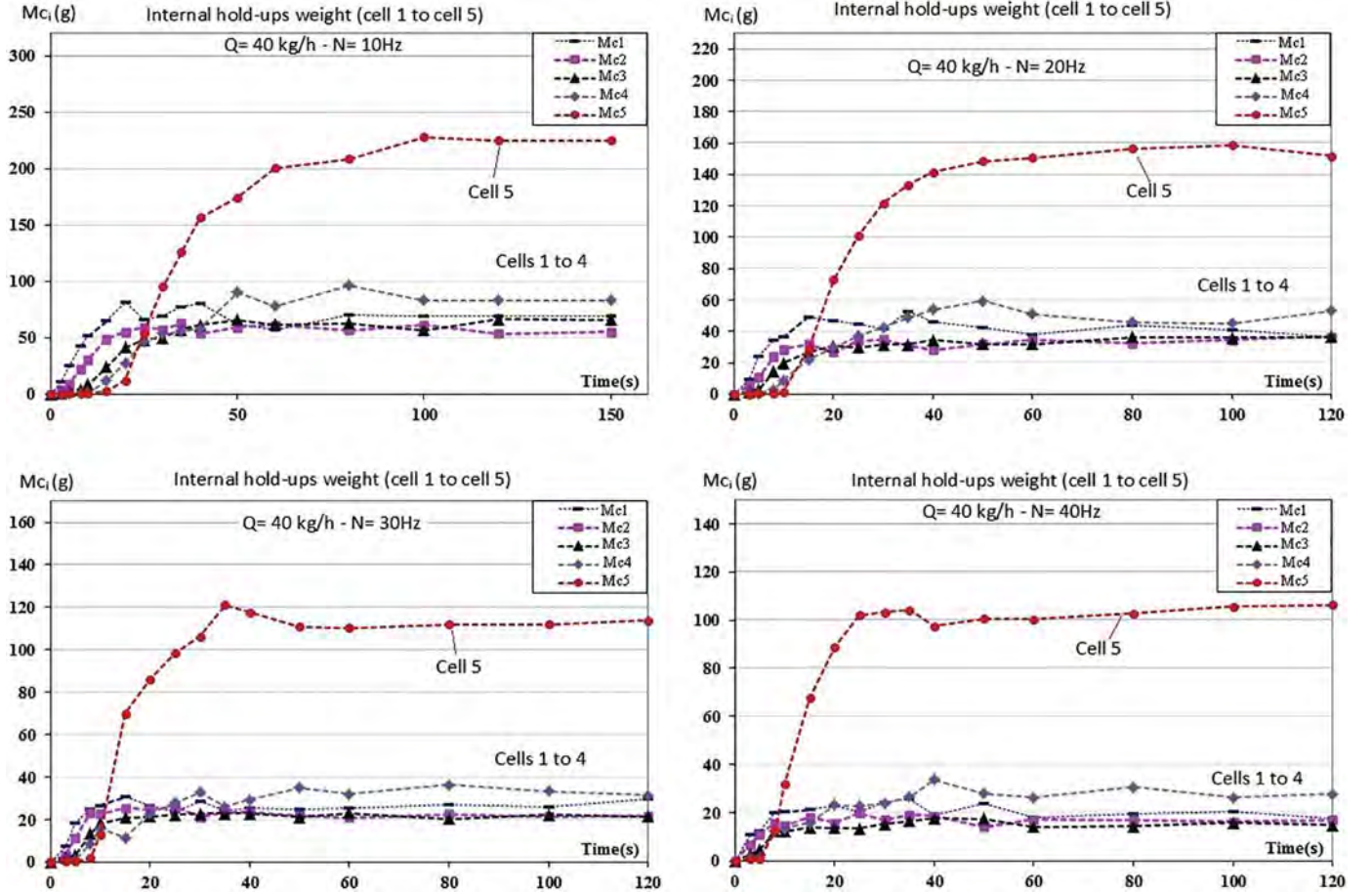


Fig. 7. Distribution of the hold-up weights alongside the mixer for different rotational speeds of the stirrer,  $Q_{in} = 40 \text{ kg h}^{-1}$ .

Therefore:

$$R = \alpha_{i-1,i} = \alpha_{i+1,i} - 1 \quad \bar{\mu}_i = \frac{Q_{in}}{M_i} \quad \text{and} \quad \bar{\mu}_1 = \frac{Q_{in}}{M_1 + \Delta F_1} \quad (17)$$

This time, the Markov chain is homogeneous and the steady-state transition matrix obtained is similar to that obtained by Tamir [46] for

a simpler case:

$$P = \begin{bmatrix} 1 - (1 + R)\bar{\mu}_1\Delta t & R\bar{\mu}_2\Delta t & \dots & 0 \\ (1 + R)\bar{\mu}_1\Delta t & 1 - (1 + 2R)\bar{\mu}_2\Delta t & \vdots & 0 \\ 0 & (1 + R)\bar{\mu}_2\Delta t & R\bar{\mu}_{n-1}\Delta t & \vdots \\ \vdots & 0 & 1 - (1 + R)\bar{\mu}_{n-1}\Delta t & 0 \\ 0 & \dots & \bar{\mu}_{n-1}\Delta t & 1 \end{bmatrix} \quad (18)$$

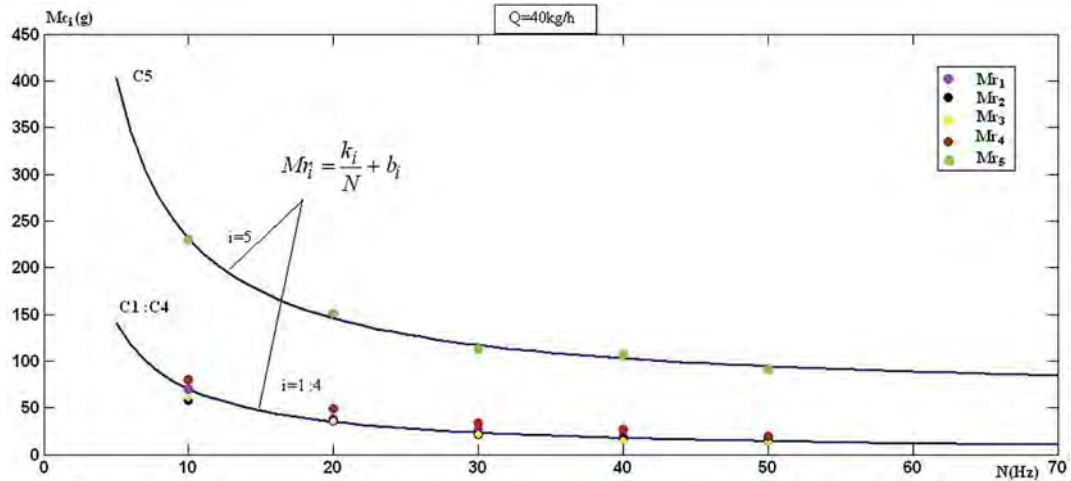


Fig. 8. Correlations obtained for the steady-state internal hold-ups as a function of the rotational speed  $N$ ,  $Q_{in} = 40 \text{ kg h}^{-1}$ .

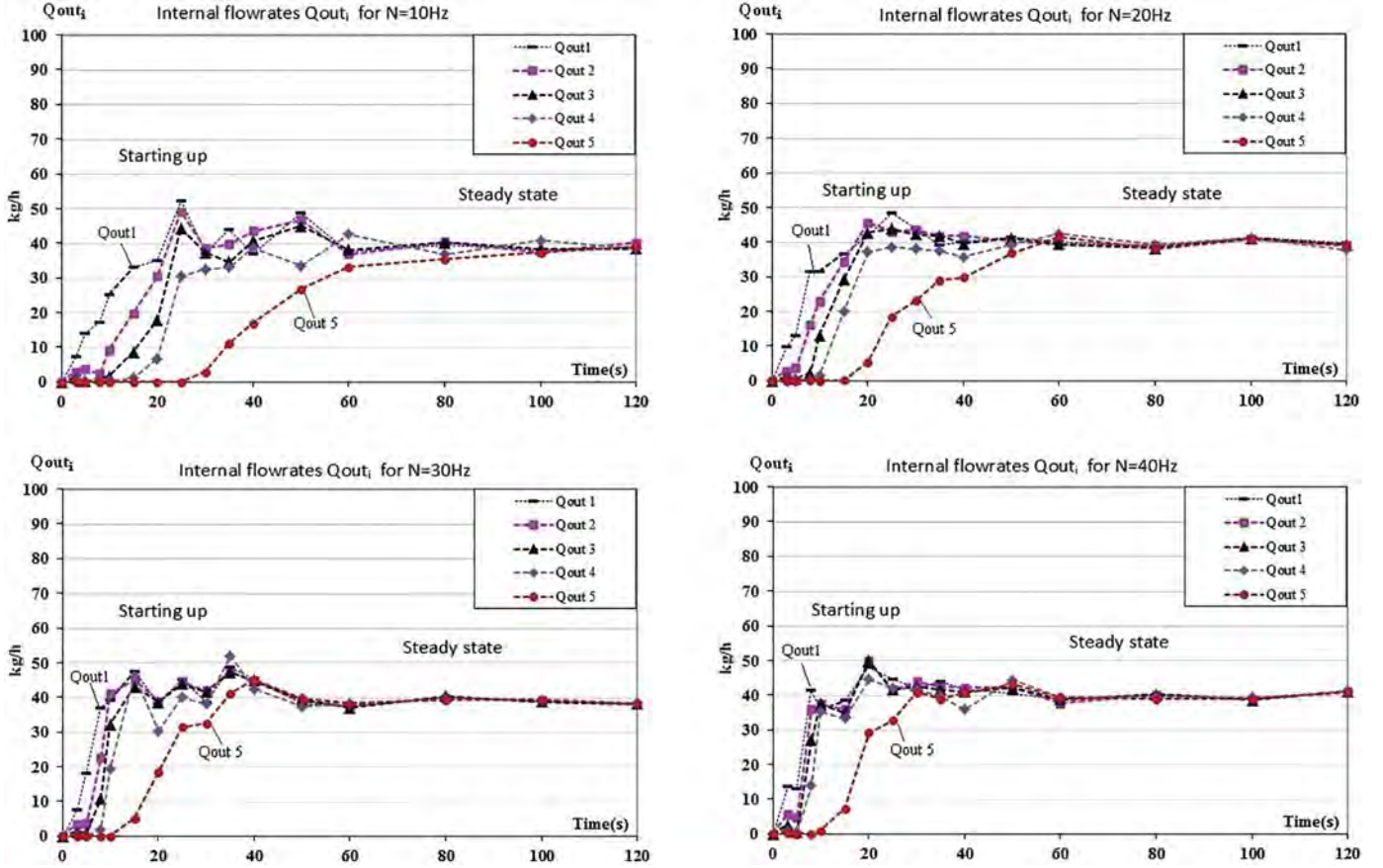


Fig. 9. Evolution of the local net flowrates during the start of the mixer for different values of  $N$ ,  $Q_{in} = 40 \text{ kg h}^{-1}$ .

### 3.3. An example of simulation

The model presented above can be used to simulate any type of flow configuration and regime, such as starting-up, emptying, tracer pulse and Residence Time Distribution curves, inlet flowrate perturbations, staged feed, etc. To illustrate its potential, we will simulate the bulk powder flow inside the mixer during the start-up phase in terms of the distribution of the hold-up weights and the evolution of the internal flowrates.

As a first approach, we will consider the homogeneous matrix of Eq. (18) for a 6 cells case (5 mixer cells + 1 absorbing) to perform the

simulations. This matrix only depends on the values of  $R$  and that of the  $\bar{\mu}_i$ , that are therefore necessary to run the model.

In Fig. 4, we can see the simulation of the time-evolution of internal hold-ups and flowrates during the start of the mixer, for two different values of  $R$  (0.5 and 10) and for  $\bar{\mu}_i = 1 \text{ s}^{-1}$  (whatever the cell  $i$ ). The inlet flowrate is set at  $Q_{in} = 40 \text{ kg h}^{-1}$  and the initial state vector is 0. Afterwards, the masses in the states of the chain are calculated thanks to Eq. (9).

For  $R = 0.5$ , the hold-ups in the cells are higher in cell  $i$  than in cell  $i + 1$ , whatever the time considered. Steady-state is obviously reached earlier for the first cells of the mixer

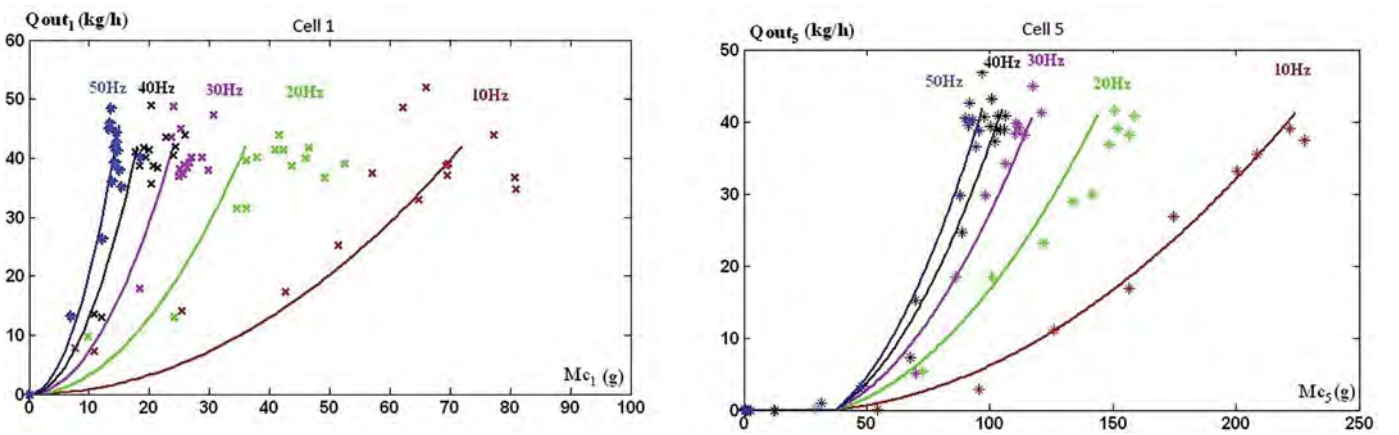


Fig. 10. Empirical link between the local net flowrates and the corresponding hold-up weights during the transitory phase (for cells 1 and 5), evidencing the existence of a minimal mass.



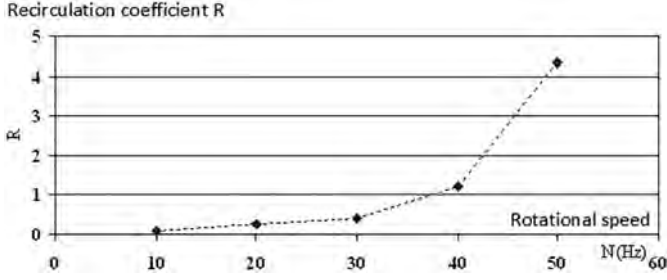


Fig. 11. Recirculation coefficients  $R$  determined by the Levenberg-Marquardt algorithm through all the experimental data available,  $Q_{in} = 40 \text{ kg h}^{-1}$ .

than for the last ones. After 15 s of simulation, all the internal masses are equal and steady-state is reached. The flowrates can be grouped according to their direction (forward for  $Q_{i+1,i}$  or backward for  $Q_{i,i+1}$ ). In each group, the flowrates corresponding to the first cells are always greater than the following ones and they attain steady-state earlier. Forward flowrates reach a steady value of  $60 \text{ kg h}^{-1}$ , while backward ones reach a  $20 \text{ kg h}^{-1}$  value, still in 15 s.

As could be expected, a high recirculation ratio ( $R = 10$ ) or back-mixing induces closer values for the hold-ups. The flowrates in the forward direction are also closer to each other, as well as those in the backward direction. The two types of flowrates are

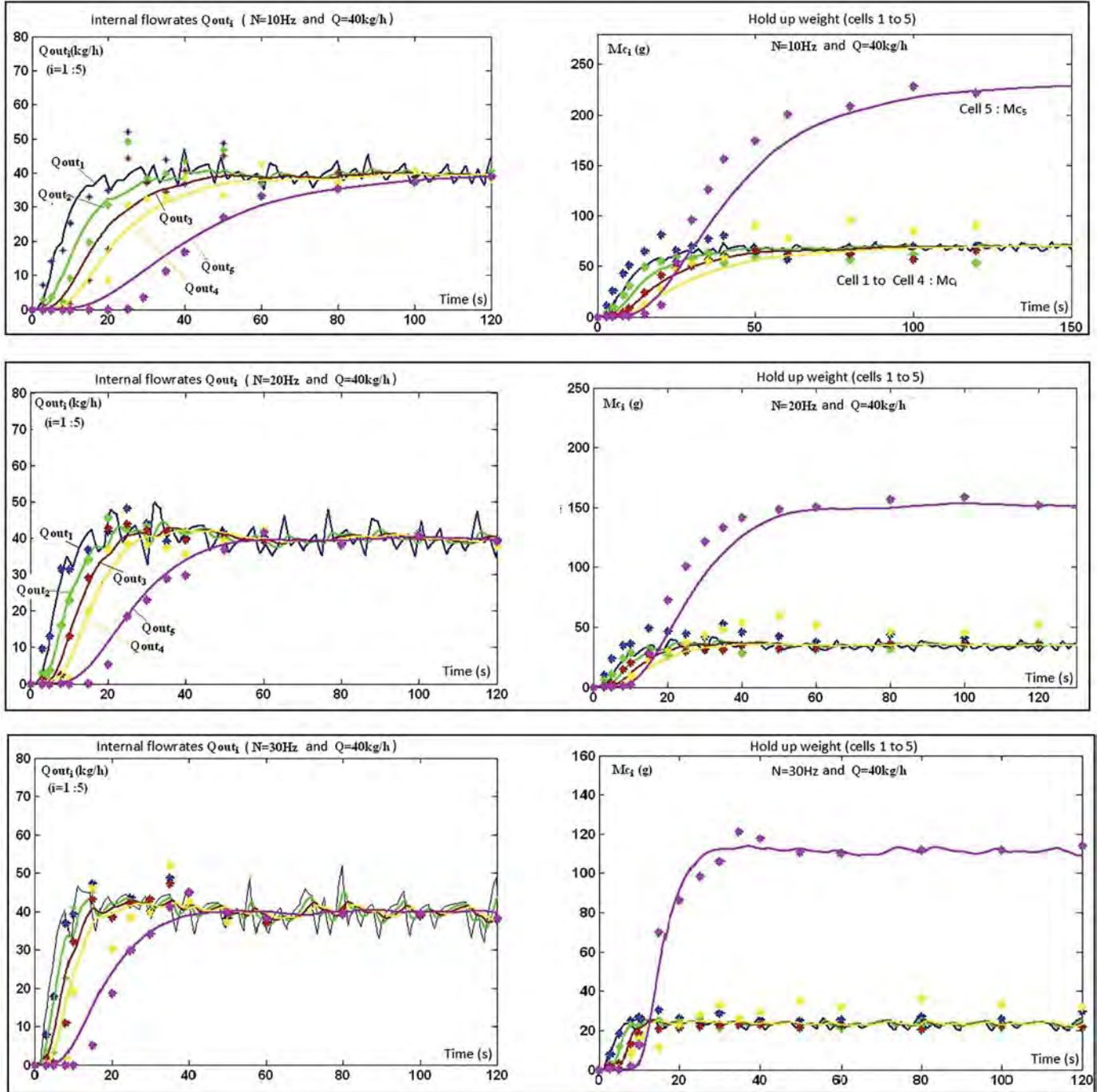


Fig. 12. Comparison of the homogeneous chain model's results with the experiments in terms of local outflow rates and internal hold-up weights during start-up, for various stirrer's rotational speeds,  $Q_{in} = 40 \text{ kg h}^{-1}$ .



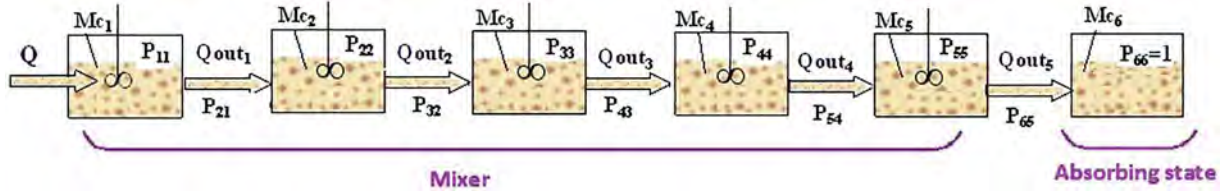


Fig. 13. Simplified Markov chain non-homogeneous model.

also closer to each other than for a much smaller recirculation ratio. Because of the high value of  $R$ , forward and backward steady-state flowrates are higher than the outlet flowrate  $Q_{out}$ , respectively 440 and 380 kg h<sup>-1</sup>. In addition, it seems that there is no influence of  $R$  on the attainment of the steady-state, which is reached after 15 s in all cases.

It is worth noting that, even if the transition matrix does not change with time because it has fixed values of  $R$  and  $\bar{\mu}_i$ , the coefficients  $\alpha_{ij}(k)$  and  $\mu_i(k)$  are changing during the transitory phase. For

instance, these are calculated at each step through:

$$\mu_i(k) = \frac{Q_{in}}{M_i(k)}, \alpha_{i+1,i}(k) = \frac{Q_{i+1,i}(k)}{Q_{in}} \text{ and } \alpha_{i-1,i}(k) = \frac{Q_{i-1,i}(k)}{Q_{in}}$$

Fig. 5 shows the evolution these parameters during the simulation, until they reach their steady values, respectively  $\bar{\mu}_i$ ,  $1 + R$  and  $R$ . Being the mixer initially empty, the  $\mu_i$ 's are infinite for  $t = 0$ , then decrease towards  $\bar{\mu}_i$ . The flowrates coefficients are all starting from zero

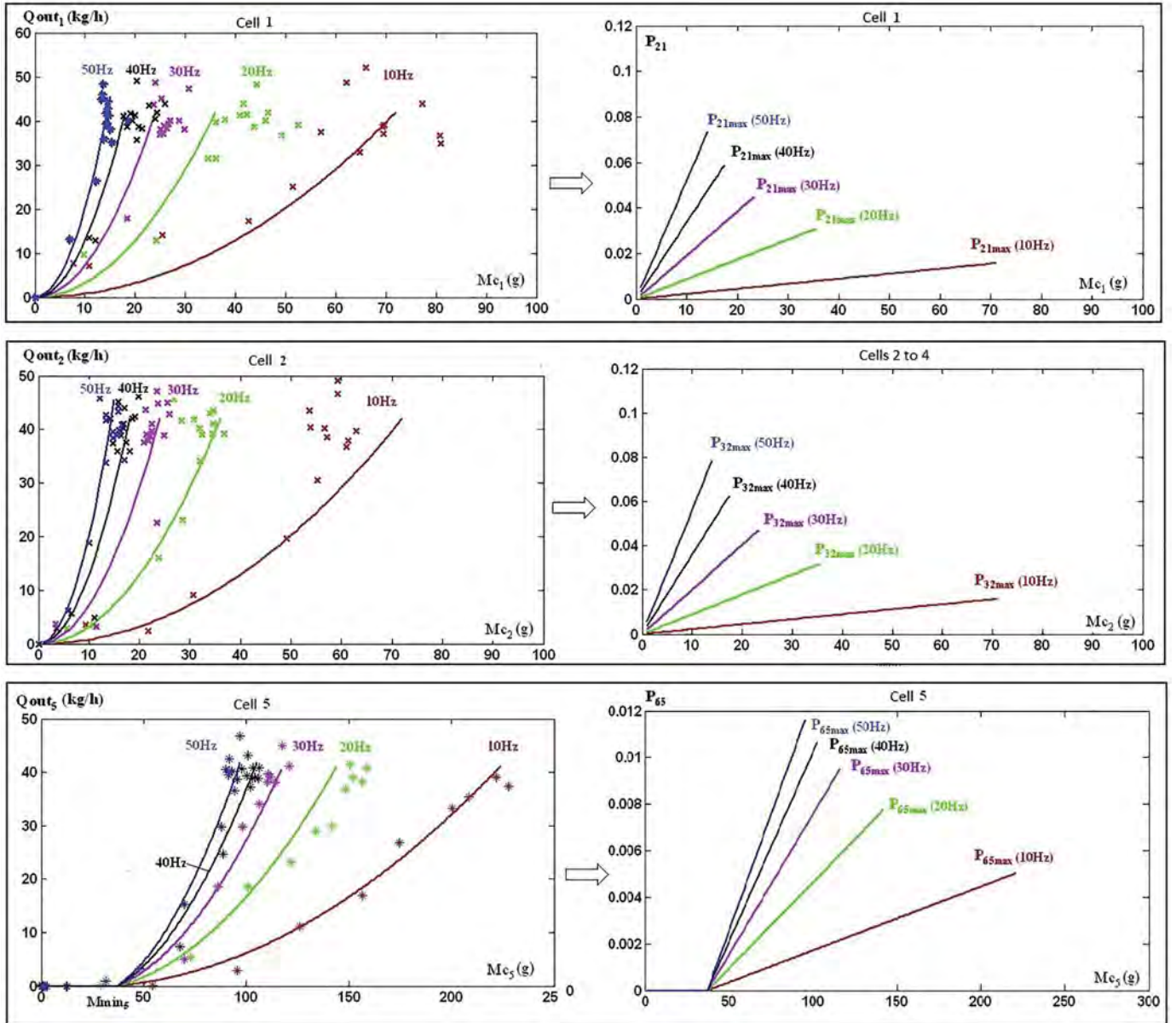
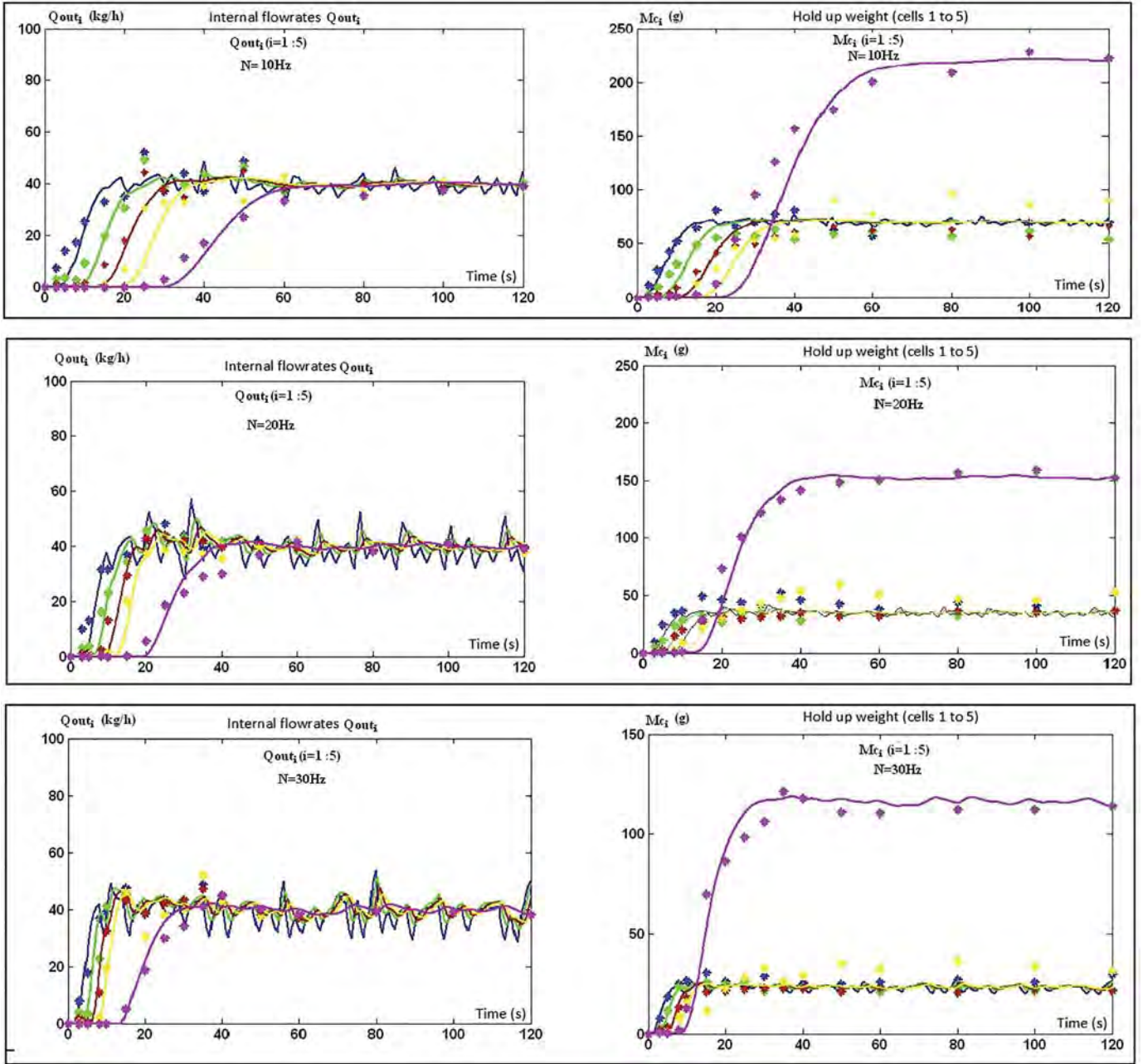


Fig. 14. Evidence of a second-order relation between internal flowrates and hold-ups during the start of the mixer, driving to a linear relation for transition probabilities,  $Q_{in} = 40$  kg h<sup>-1</sup>,  $\Delta t = 0.1$  s.



**Fig. 15.** Comparison of the non-linear chain model's results with the experiments in terms of local outflow rates and internal hold-up weights during start-up, for various stirrer's rotational speeds,  $Q_{in} = 40 \text{ kg h}^{-1}$ .

(no initial flow) and increase towards their steady values, depending on whether they are concerned with forward flow or backward flow. The coefficient  $\alpha_{6,5}$  depicts the flow from the last cell to the outlet divided by the steady outlet flow, its steady value is therefore equal to 1. This procedure can also be used to describe the process evolution during a step change in operating conditions, such as the stirrer's speed  $N$ . In Fig. 6, internal hold-ups, as well as the outflow rate evolutions are plotted after a step change from a value  $N_1$  to a value  $N_2$ , which may correspond to the change from a matrix  $P_1$  to a matrix  $P_2$ . In this example, the pair  $(R, \mu_i)$  changes from  $(1, 0.2)$  to  $(10, 1)$ . Because the mixer is already at steady-state, the impact of the perturbation on the hold-ups is a global quick decrease of all the values to the new situation. The outflow rate experiences a strong perturbation through a peak that is close to 5 times  $Q_{in}$ , before getting back to this nominal value. This is due to the fact that  $R$  is instantly placed at a much higher value, which in turn forces particles to flow out of the equipment.

#### 4. Single product bulk flow modelling

##### 4.1. Internal hold-up weights and flow rates

The coarse product (coarse couscous) has been first investigated in terms of internal flows and mass distribution inside the blender. Fig. 7 shows the distribution of the hold-up weights measured experimentally in each of the 5 cells defined, for the flowrate  $Q_{in} = 40 \text{ kg h}^{-1}$  and rotational speeds varying between 10 and 40 Hz. Cells are experiencing a filling process one after another which is due to the chain construction. The masses in cells 1, 2, 3 and 4 follow identical trends, leading to a steady mass which is approximately the same whatever the cell.

In cell 5, which corresponds to the last mixing section before mixer's outlet, the powder mass is much higher, nearly five times that of the other cells. This is due to presence of the mixer's wall that corresponds



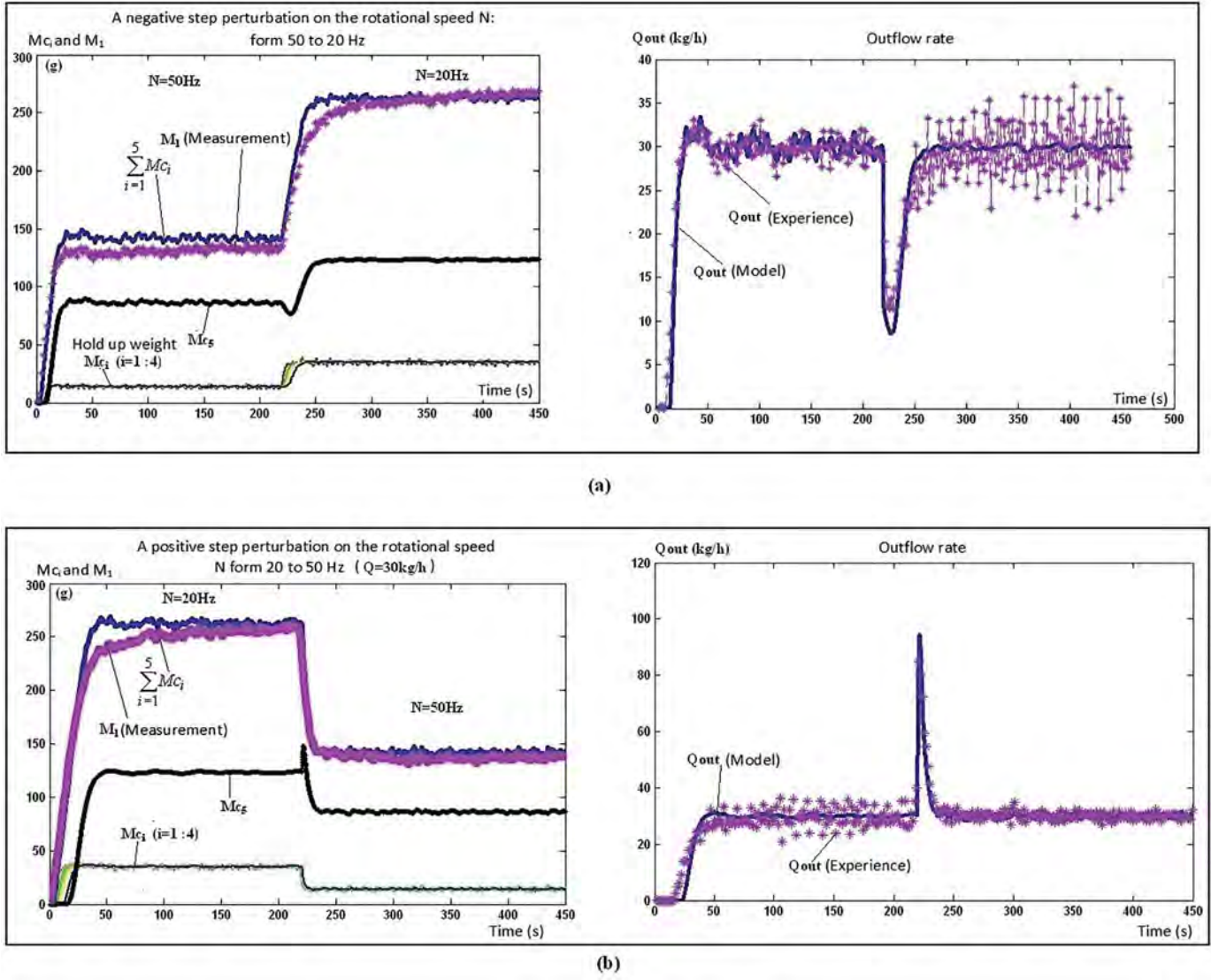


Fig. 16. Comparison of the non-linear chain model's results with the experiments in terms of hold-up and outflow rate, during either a positive or a negative step perturbation of the stirrer's rotational speed (from 20 to 50 Hz and vice-versa),  $Q_{in} = 30 \text{ kg h}^{-1}$ .

to an outlet section which is much smaller than the section of the flow in the previous cells. More than half of the powder in the mixer is indeed in the last part of it, close to the outlet. The good mixing of this section is therefore critical.

For what concerns the impact of  $N$ , it can be seen that, at a fixed  $Q_{in}$ , the higher the speed, the smaller the hold-ups in every cells, which is not surprising. The steady-state values  $\bar{M}_i$  of the hold-ups can be plotted against  $N$  (Fig. 8) and drive to the following empirical correlations after least square fitting of curves of the form  $M_i = a_i/N + b_i$ :

$$\bar{M}_i(g) = \frac{703}{N} \text{ for } i = 1 \text{ to } 4 \quad \bar{M}_5(g) = \frac{1714}{N} + 60 \quad (19)$$

The data collected also allows for the determination of the local net flowrates in the forward direction  $\Delta Q_{i+1,i}$  at any time and for each cell by comparing the masses after a small time interval  $\Delta t$ :

$$\Delta Q_{i+1,i} = Q_{i+1,i} - Q_{i,i+1} = \frac{\sum_{j=i+1}^6 [M_j(t + \Delta t) - M_j(t)]}{\Delta t} \quad (20)$$

The time evolution of these flowrates during the mixer's start is presented in Fig. 9. Each of these intermediary flowrates increases at a rate that is dependent on the rotational stirrer's speed  $N$ : as expected, higher

values of  $N$  drive to a quicker establishment of a steady-state. The steady value of the flowrates is the same whatever the cell considered, and is equal to the inflow rate  $Q_{in}$  (which is  $40 \text{ kg h}^{-1}$  in the present case). Contrarily to what happens in the other cells, it can be noted that the outflow rate  $Q_{5,6}$ , which is also that of the mixer  $Q_{out}$ , only increases after a minimal mass of approximately 40 g is attained in cell 5. This result is emphasized in Fig. 10, which represents  $\Delta Q_{i+1,i}$  as a function of  $M_i$  for cells 1 and 5, from which the following empirical correlation can be drawn and is valid during the transitory phase:

$$\Delta Q_{i+1,i}(k) = aM_i^2(k) + bM_i(k) + c \quad (21)$$

Where  $a$ ,  $b$  and  $c$  are parameters depending on  $N$ .

#### 4.2. Homogeneous model

In this section, we will first consider the homogeneous model presented above, which means that the transition matrix  $P$  is that of (Eq. (18)).  $P$  depends on six parameters, the five values of  $\bar{\mu}_i$  and  $R$ . The  $\bar{\mu}_i$ 's are available from both  $Q_{in}$  and the steady hold-up weight in each cell  $i$ . As this is in turn linked to  $N$  through (Eq. (19)), we have a general relationship of  $\bar{\mu}_i$  vs  $N$ . For the parameter  $R$ , we will proceed

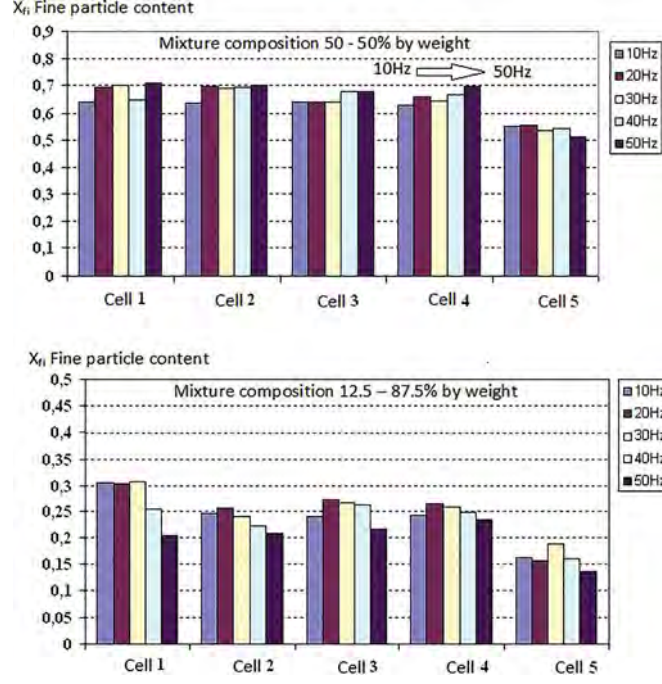


Fig. 17. Fine particle content inside the mixer as measured for mixture 1 (top) and mixture 2 (bottom), evidencing a segregation phenomenon,  $Q_{in} = 40 \text{ kg h}^{-1}$ .

to an optimization scheme ruled by a Levenberg-Marquardt algorithm run on Matlab®, through minimalizing the following criteria D based on the internal hold-up weights:

$$D = \sum_{j=1}^5 \sum_{i=1}^{n_{exp}} \left\{ [M_j(i)]_{model} - [M_j(i)]_{exp} \right\}^2 \quad (22)$$

In the above equation,  $n_{exp}$  is the number of experimental data considered.

This has been repeated for each rotational stirrer's speed and is plotted on Fig. 11. As expected, R increases with N through what may be viewed as a power law, which is consistent with previous works on RTD in such mixers [28].

As explained in the example of simulation with this model, while the transition matrix does not vary with time, it can serve to calculate the evolution of the system during the transitory phases, such as the mixer's start through (Eq. (9)). Fig. 12 shows the comparison of model and experiments in terms of internal hold-up weights  $M_i(t)$  (to which R has been fitted) and local net flowrates  $\Delta Q_{i+1,i}(t)$  which is derived from the  $M_i(t)$ 's.

Being the chain homogeneous, it is not surprising to see that the model results are all the more acceptable that the flow regime is at steady-state. Steady values of the flowrates and the hold-ups are well predicted by the model, whatever the rotational stirrer's speed is. While the model is still able to capture the global behaviors during the start of the mixer it fails in a fine description of the evolution of the hold-ups, in particular for cell 5. The outflow rate of the mixer  $\Delta Q_{6,5}$  is also not well predicted. The model forces the particles to flow out of the equipment since the beginning of the run, while it has been recorded that a minimal mass  $M_{min,5}$  in cell 5 was necessary for that to happen.

#### 4.3. Non-homogeneous model

In the previous homogeneous model, the main difficulty came from the impossibility to measure or calculate all the flowrates  $Q_{ij}$ , but only net flow rates  $\Delta Q_{i+1,i}$ . For this, we now consider a simplified Markov chain model for which the exchanges between adjacent cells are replaced by these net flow rates. By doing so, we have:  $\Delta Q_{i+1,i} = Q_{i+1,i}$ .

This model (see Fig. 13) can be viewed as a series of continuous stirred tank reactors (CSTRs). The fact that no back-mixing is permitted is consistent with the data obtained on the hold-ups, the real mixing section being finally cell 5. As a result, the general matrix rule for the calculation of the internal hold-up weights, and subsequent outflow rates, will be:

$$\begin{bmatrix} M_1(k+1) \\ M_2(k+1) \\ M_3(k+1) \\ M_4(k+1) \\ M_5(k+1) \\ M_6(k+1) \end{bmatrix} = \begin{bmatrix} p_{1,1}(k) & 0 & 0 & 0 & 0 & 0 \\ p_{2,1}(k) & p_{2,2}(k) & 0 & 0 & 0 & 0 \\ 0 & p_{3,2}(k) & p_{3,3}(k) & 0 & 0 & 0 \\ 0 & 0 & p_{4,3}(k) & p_{4,4}(k) & 0 & 0 \\ 0 & 0 & 0 & p_{5,4}(k) & p_{5,5}(k) & 0 \\ 0 & 0 & 0 & 0 & p_{6,5}(k) & p_{6,6}(k) \end{bmatrix} \begin{bmatrix} M_1(k) + \Delta F_1(k) \\ M_2(k) \\ M_3(k) \\ M_4(k) \\ M_5(k) \\ M_6(k) \end{bmatrix} \quad (23)$$

As for (Eqs. (15)–(16)), the transition probabilities can be derived from the internal hold-up weights and flowrates:

$$\begin{aligned} p_{21}(k) &= \frac{Q_{21}(k)\Delta t}{M_1(k) + \Delta F_1(k)} & p_{11}(k) &= 1 - \frac{Q_{21}(k)\Delta t}{M_1(k) + \Delta F_1(k)} & \text{for cell 1} \\ p_{i+1,i}(k) &= \frac{Q_{i+1,i}(k)\Delta t}{M_i(k)} & p_{ii}(k) &= 1 - \frac{Q_{i+1,i}(k)\Delta t}{M_i(k)} & \text{for cells 2 to 5} \end{aligned} \quad (24)$$

In Fig. 14, the flowrates  $Q_{ij}(k)$  measured inside the mixer are plotted against the corresponding hold-up weights, for cells 1, 2 and 5, as well as for different values of N. Second-order correlations fits the data very well if the minimum mass  $M_{min,5}$  is considered, which means that the



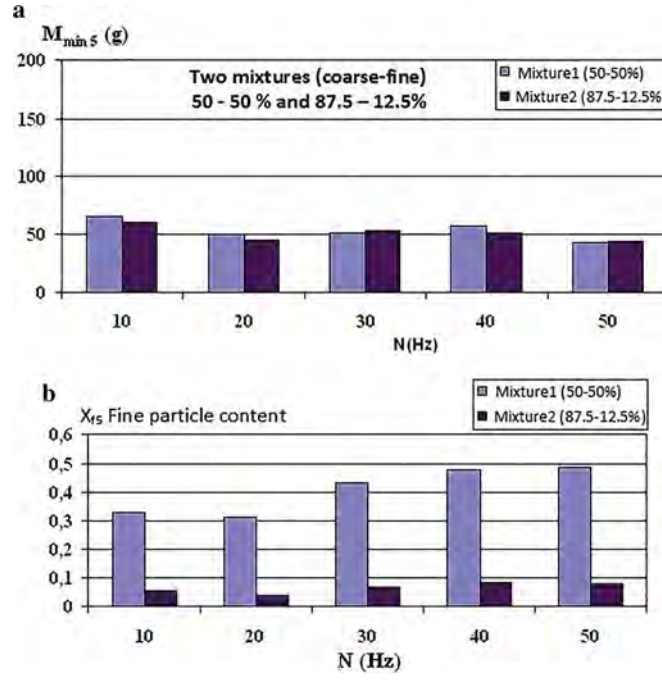


**Fig. 18.** (a) Evidence of the equality of the minimal masses in cell 5 (a); (b) fine particles content of the minimal mass in cell 5 according the various operational conditions considered (b),  $Q_{in} = 40 \text{ kg h}^{-1}$ .

transition probabilities are following linear relationships with  $M_i(k)$ :

$$i = 1 : Q_{21}(k) = a_1 M_1(k)(M_1(k) + \Delta F_1(k)); p_{21}(k) = a_1 M_1(k) \Delta t \quad (25)$$

$$i = 2, 3, 4 : Q_{i+1,i}(k) = a_i M_i(k)^2; p_{i+1,i}(k) = a_i M_i(k) \Delta t \quad (26)$$

$$i = 5 : Q_{65}(k) = a_5 M_5(k)(M_5(k) - M_{min,5}); p_{65}(k) = a_5 (M_5(k) - M_{min,5}) \Delta t \quad (27)$$

It must be noted that when  $M_5(k)$  is smaller than  $M_{min,5}$ ,  $Q_{65} = 0$  and  $p_{65}(k) = 0$ . The Fig. 14 also shows the plots of  $p_{i+1,i}(k)$  as a function of  $M_i(k)$ , confirming the above development.

The set of equations (Eqs. (25)–(27)) demonstrates that, as long as the internal hold-ups are evolving with time, such as during a transitory phase, the transition matrix depends on the actual state of the system. This means that the Markov chain is not only non-homogeneous, but also non-linear. When the hold-ups are steady, transition probabilities are all establishing themselves at a fixed value  $p_{ij,max}$ , for which internal flowrates are replaced by  $Q_{in}$ , the chain becoming then homogeneous:

$$p_{21,max} = \frac{Q_{in} \Delta t}{M_1 + Q_{in} \Delta t} \quad p_{i+1,i,max} = \frac{Q_{in} \Delta t}{M_i} \quad (\text{for cells 2 to 5}) \quad (28)$$

The maximum values of the probabilities can be extracted graphically from Fig. 14, and used to determine the parameters  $a_i$ :

$$a_1 = \frac{p_{21,max}}{M_1} \quad a_i = \frac{p_{i+1,i,max}}{M_i} \quad (i = 2, 3, 4) \quad a_5 = \frac{p_{65,max}}{M_5 - M_{min,5}} \quad (29)$$

If a new perturbation takes place, such as change in stirrer's rotational speed or mixer's emptying process, the hold-ups will change

towards their corresponding steady value. This will in turn affect the probabilities and the homogeneity of the Markov chain.

Fig. 15 shows the results obtained by the new model, as compared to the experimental results measured in terms of internal flowrates and hold-ups during the start of the mixer, for various rotational stirrer's speed. The model captures all these variations very well, in particular for the mixer's outflow rate that was not well predicted by the previous homogeneous chain. The small discrepancies that can be noted for  $N = 10 \text{ Hz}$  can be attributed to the lack of stability of the speed itself.

To test the model a bit farther, negative and positive step perturbations on the stirrer's rotational speed have been imposed to the system after it has reached steady-state, both experimentally and numerically. The results are presented in Fig. 16 in terms of hold-up weights (within cells or global) and outflow rate of the mixer. The model proves here that it follows extremely well the strong perturbations during its occurrence, as well as it succeeds in predicting the new stable regime.

## 5. Binary mixture flow modelling

### 5.1. Derivation of a non-homogeneous model

To model the flow of a binary mixture that consists of coarse and fine particles, we will consider that each type of particle is following a Markov chain on its own. We therefore have two transition matrices  $P_c(k)$  and  $P_f(k)$  that correspond to the coarse particles and the fine particles respectively, made of transition probabilities  $p_{cij}(k)$  and  $p_{fij}(k)$ , but also states vectors  $M_c(k)$  and  $M_f(k)$ , each consisting of the masses  $M_{ci}(k)$  and  $M_{fi}(k)$  in the 6 cells defined above, as well as inlet masses  $\Delta F_c(k)$  and  $\Delta F_f(k)$ . After  $k$  transitions, the particle flow is

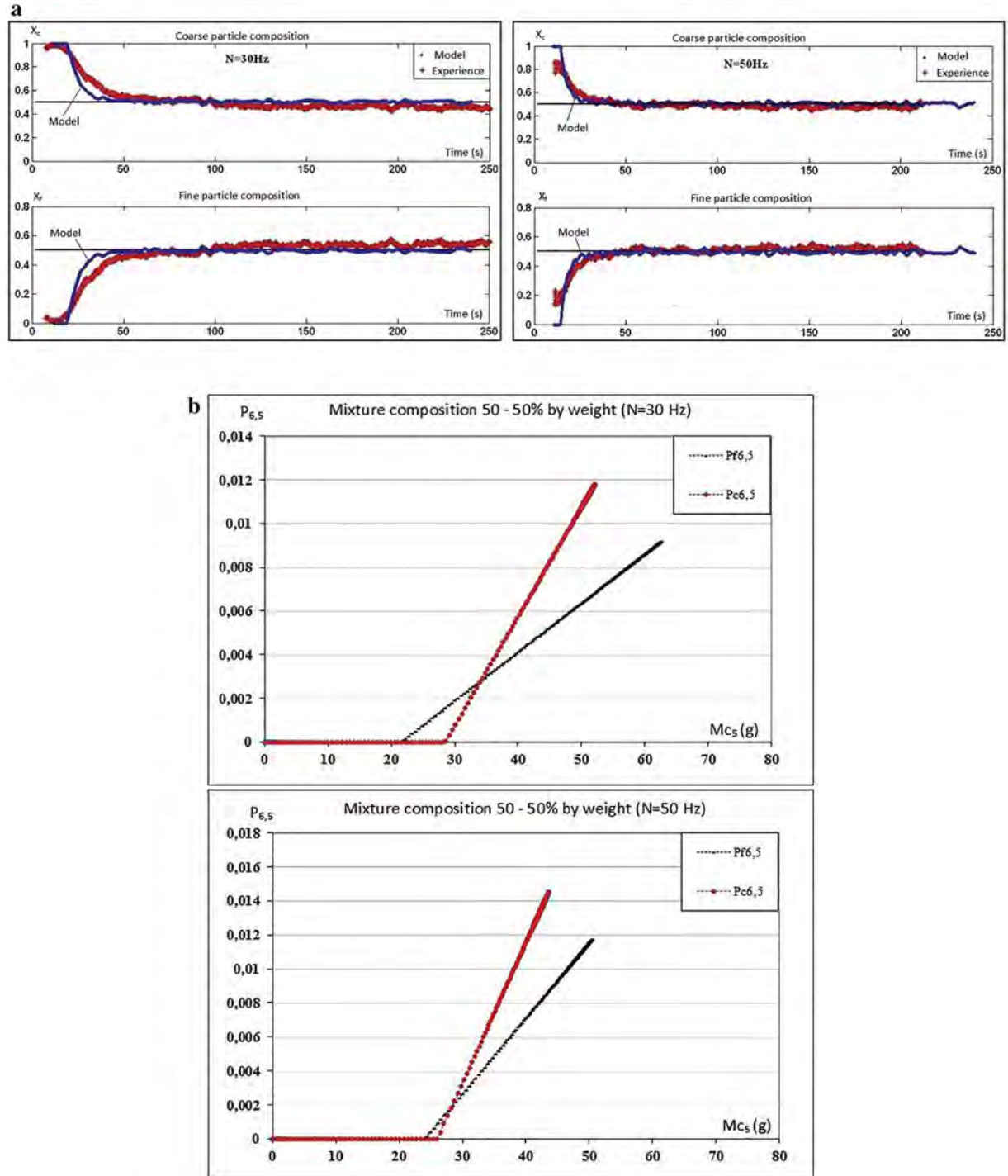


**Fig. 19.** Simulation of mixer start, mixture 1, two different values of  $N$  - (a) Comparison of the Markov chain model's results with the experiments in terms of outflow composition; (b)  $p_{6,5} - M_5$  probability plots,  $Q_m = 40\text{ kg h}^{-1}$ ,  $\Delta t = 0,1\text{ s}$ .

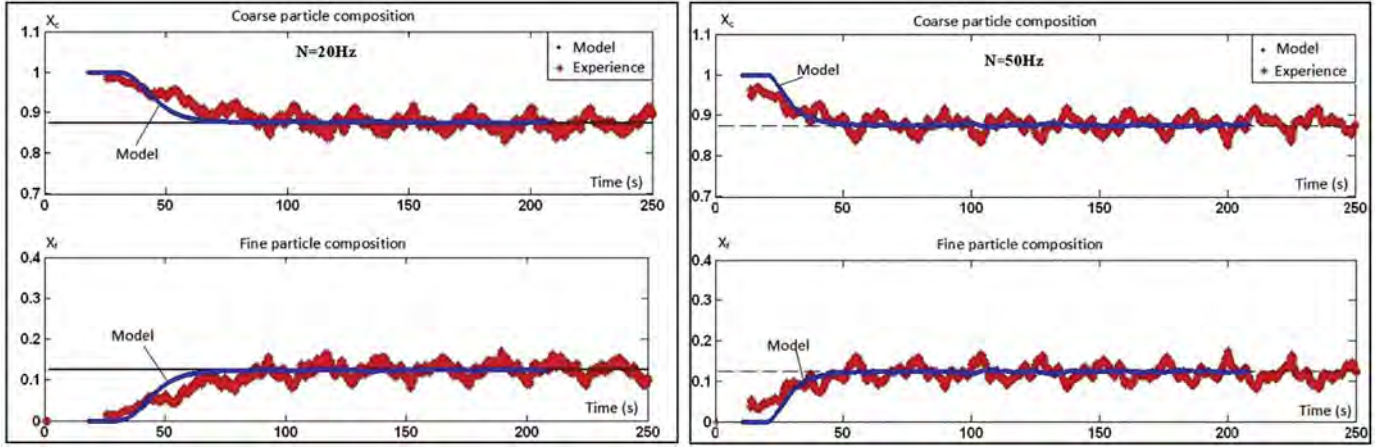


**Fig. 20.** Simulation of mixer start, mixture 2, two different values of  $N$  - Comparison of the Markov chain model's results with the experiments in terms of outflow composition,  $Q_{in} = 40 \text{ kg h}^{-1}$ ,  $\Delta t = 0,1 \text{ s}$ .

therefore ruled by the following equations:

$$\begin{bmatrix} M_{c1}(k+1) \\ M_{c2}(k+1) \\ M_{c3}(k+1) \\ M_{c4}(k+1) \\ M_{c5}(k+1) \\ M_{c6}(k+1) \end{bmatrix} = \begin{bmatrix} p_{c1,1}(k) & 0 & 0 & 0 & 0 & 0 \\ p_{c2,1}(k) & p_{c2,2}(k) & 0 & 0 & 0 & 0 \\ 0 & p_{c3,2}(k) & p_{c3,3}(k) & 0 & 0 & 0 \\ 0 & 0 & p_{c4,3}(k) & p_{c4,4}(k) & 0 & 0 \\ 0 & 0 & 0 & p_{c5,4}(k) & p_{c5,5}(k) & 0 \\ 0 & 0 & 0 & 0 & p_{c6,5}(k) & p_{c6,6}(k) \end{bmatrix} \begin{bmatrix} M_{c1}(k) + \Delta F_{c1}(k) \\ M_{c2}(k) \\ M_{c3}(k) \\ M_{c4}(k) \\ M_{c5}(k) \\ M_{c6}(k) \end{bmatrix}$$

$$\begin{bmatrix} M_{f1}(k+1) \\ M_{f2}(k+1) \\ M_{f3}(k+1) \\ M_{f4}(k+1) \\ M_{f5}(k+1) \\ M_{f6}(k+1) \end{bmatrix} = \begin{bmatrix} p_{f1,1}(k) & 0 & 0 & 0 & 0 & 0 \\ p_{f2,1}(k) & p_{f2,2}(k) & 0 & 0 & 0 & 0 \\ 0 & p_{f3,2}(k) & p_{f3,3}(k) & 0 & 0 & 0 \\ 0 & 0 & p_{f4,3}(k) & p_{f4,4}(k) & 0 & 0 \\ 0 & 0 & 0 & p_{f5,4}(k) & p_{f5,5}(k) & 0 \\ 0 & 0 & 0 & 0 & p_{f6,5}(k) & p_{f6,6}(k) \end{bmatrix} \begin{bmatrix} M_{f1}(k) + \Delta F_{f1}(k) \\ M_{f2}(k) \\ M_{f3}(k) \\ M_{f4}(k) \\ M_{f5}(k) \\ M_{f6}(k) \end{bmatrix}$$

Obviously, the hold-up weight  $M_i(k)$  and the composition  $X_{fi}(k)$  in fine particles in cell  $i$  are given by:

$$M_i(k) = M_{ci}(k) + M_{fi}(k) \quad X_{fi}(k) = \frac{M_{fi}(k)}{M_{ci}(k) + M_{fi}(k)} \quad (32)$$

In particular, the outlet composition of the mixture can be calculated through (note  $Q_{fij}$  and  $Q_{mij}$  are the local net flow rates in fine and coarse particles respectively):

$$X_f(k) = \frac{Q_{f65}(k)}{Q_{c65}(k) + Q_{f65}(k)} = \frac{p_{f6,5}(k)M_{f5}(k)}{p_{f6,5}(k)M_{f5}(k) + p_{c6,5}(k)M_{c5}(k)} \quad (33)$$

$$X_c(k) = \frac{Q_{c65}(k)}{Q_{c65}(k) + Q_{f65}(k)} = \frac{p_{c6,5}(k)M_{c5}(k)}{p_{f6,5}(k)M_{f5}(k) + p_{c6,5}(k)M_{c5}(k)} \quad (34)$$

Because the same equations hold for either the coarse or the fine particles, we will limit our analysis to the fine product.

As for the bulk flow model, the transition probabilities are linked to the flow and masses through:

$$p_{f21}(k) = \frac{Q_{f21}(k)\Delta t}{M_{f1}(k) + \Delta F_{f1}(k)} \quad \text{for cell 1; } p_{fi+1,i}(k) = \frac{Q_{fi+1,i}(k)\Delta t}{M_{fi}(k)} \quad \text{for cells 2 to 5} \quad (35)$$

When steady-state is reached, probabilities are assigned to their steady values. So if  $\bar{M}_{fi}$  is the steady hold-up in cell  $i$ , those maximum probabilities are:

$$(p_{f21})_{max} = \frac{Q_{f21}\Delta t}{\bar{M}_{f1} + Q_{f21}\Delta t} \quad (p_{fi+1,i})_{max} = \frac{Q_{fi+1,i}\Delta t}{\bar{M}_{fi}} \quad \text{for cells 2 to 5} \quad (36)$$

We further assume a linear relationship between the probabilities and hold-ups by the introduction of constants  $a_{fi}$  that can be linked to the steady-state probabilities:

$$p_{fi+1,i}(k) = a_{fi}M_{fi}(k) \quad \text{for cells 1 to 4} \quad (37)$$

$$p_{f6,5}(k) = a_{f5}[\bar{M}_{f5}(k) - M_{f_{min,5}}(k)] \quad \text{for cell 5}$$

$$a_{f1} = \frac{Q_{f21}\Delta t}{\bar{M}_{f1}[\bar{M}_{f1} + Q_{f21}\Delta t]} \quad a_{fi} = \frac{Q_{fi+1,i}\Delta t}{\bar{M}_{fi}^2}$$

$$a_{f5} = \frac{Q_{f6,5}\Delta t}{\bar{M}_{f5}[\bar{M}_{f5} - M_{f_{min,5}}(k)]}$$

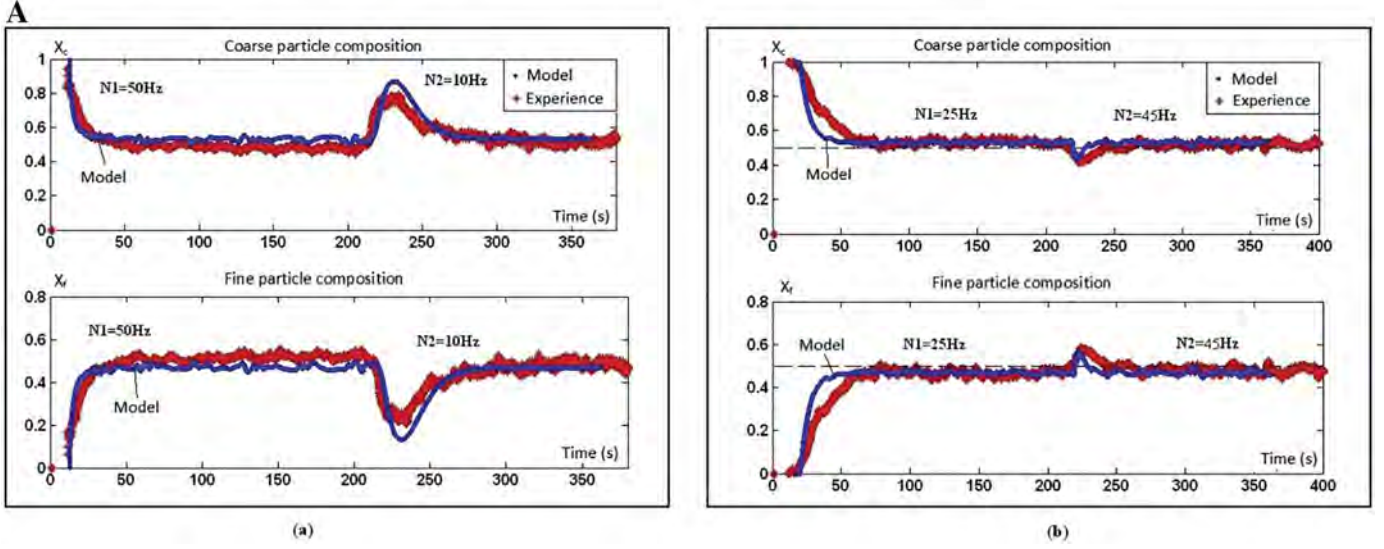


**Fig. 21.** Simulation of negative and positive perturbation steps, mixture 1 - (a) Comparison of the Markov chain model's results with the experiments in terms of outflow composition; (b)  $p_{65} - M_5$  probability plots,  $Q_{in} = 40 \text{ kg h}^{-1}$ ,  $\Delta t = 0,1 \text{ s}$ .

The last step is to transform these equations into a probability-based set of equations that demonstrates the non-homogeneous and non-linear character of the Markov chain:

$$\begin{aligned}
 p_{f21}(k) &= \frac{Mf_1(k)Qf_{in}\Delta t}{Mf_1[Mf_1 + Qf_{in}\Delta t]} \\
 p_{fi+1,i}(k) &= \frac{Mf_i(k)Qf_{in}\Delta t}{Mf_i^2} \\
 p_{f65}(k) &= \frac{[Mf_5(k) - Mf_{min,5}]Qf_{in}\Delta t}{Mf_5[Mf_5 - Mf_{min,5}]}
 \end{aligned} \quad (38)$$

## 5.2. Internal hold-up weights

For the matrix calculation of the states to be performed, the knowledge of the steady-state values of the internal hold-ups, as well as that of the minimal mass in cell 5 must be known. For this, experiments of determination of internal hold-up weights have been performed for each product during their mixing, as described earlier for the single product. The content of each cell has been withdrawn from the blender at different moments of time and sieved so as to separate coarse and fine couscous, afterward each product could be weighed. This procedure has been repeated until the steady-state regime has been reached. Two cases have been investigated, namely a 50–50% by weight mixture and a 87.5 coarse - 12.5 fine % by weight mixture. These two mixtures will further be identified by mixture 1 and mixture 2 respectively.

Fig. 17 shows the fine particle content in the five cells at steady-state for the two mixtures. As commented in Ammarcha et al. [3], the first four cells are richer in fine particles than the last cell, whatever the conditions under which the blender operates, pointing out the presence of a segregation effect. As for the coarse product alone, it can be shown that the steady hold-up weight of the mixture in each cell can be assimilated to that of coarse couscous, which means that (Eq. (19)) holds true. This allows for the determination of the steady hold-up weights of each component in every cell  $\overline{Mf}_i$  and  $\overline{Mc}_{ci}$  through the empirical relations:

$$\overline{Mf}_i = X_{fi} * \frac{703}{N} \text{ (g)}, \overline{Mc}_{ci} = (1 - X_{fi}) * \frac{703}{N} \text{ (g)} \text{ for } i = 1 \text{ to } 4 \quad (39)$$

$$\overline{Mf}_5 = X_{f5} * \left( \frac{1714}{N} + 60 \right) \text{ (g)}, \overline{Mc}_5 = (1 - X_{f5}) * \left( \frac{1714}{N} + 60 \right) \text{ (g)} \quad (40)$$

The minimal mass of each product has been also determined experimentally by stopping the mixer when the first particles begin to flow out of it, withdrawing the content of cell 5, sieve it and weigh the separated components. Fig. 18a shows that the overall minimal mass in cell 5 can be assumed to be a constant equal to 50 g, while Fig. 18b shows that the content in fine particles depends on  $N$ , in particular for mixture 1. As expected, a higher value of  $N$  drives to a mixture that is closer to the nominal value of 50% by weight for this mixture. For mixture 2, a segregated mixture is still present in the last cell, but its composition will change as steady-state is approached.

## 5.3. Binary mixing model validation

The validation of the model has been performed by comparing its results in terms of outlet's mixture composition to the measurements that have been obtained through on-line image analysis. This evaluation is based on two process operations: the start of the blender towards the attainment of steady-state and negative/positive step perturbations on the stirrer's rotational speed.

Fig. 19a presents model and experimental results obtained during the starting phase of the equipment for two stirrer's rotational speeds, for mixture 1. In both cases, the model catches the evolution of the composition very well. In particular, it predicts the fact that the mixture is richer in coarse particles during the start of the mixer, a segregation phenomenon we discussed in a recent work [3]. Fig. 19b shows the linear relationships between the evolving probabilities and the hold-up weights for cell 5 and for both component. As commented before, the probabilities are increasing with the hold-up until they reach their steady value, afterwards the calculation rule become that of an homogeneous chain. In addition, it can be seen that the minimum mass of powder that allows the outflow of the mixture, and can be estimated by adding the hold-up weights in cell 5 for each component, is roughly the same whatever the stirrer's speed and equal to 50 g. Finally, and as expected, the higher the stirrer's speed, the higher the probability for the particles to get out of the equipment. Results corresponding to mixture 2 are presented in Fig. 20. Once again, the model reproduces the experiment quite well but is unable to catch the small-scale mass fluctuations that have been recorded for each component.



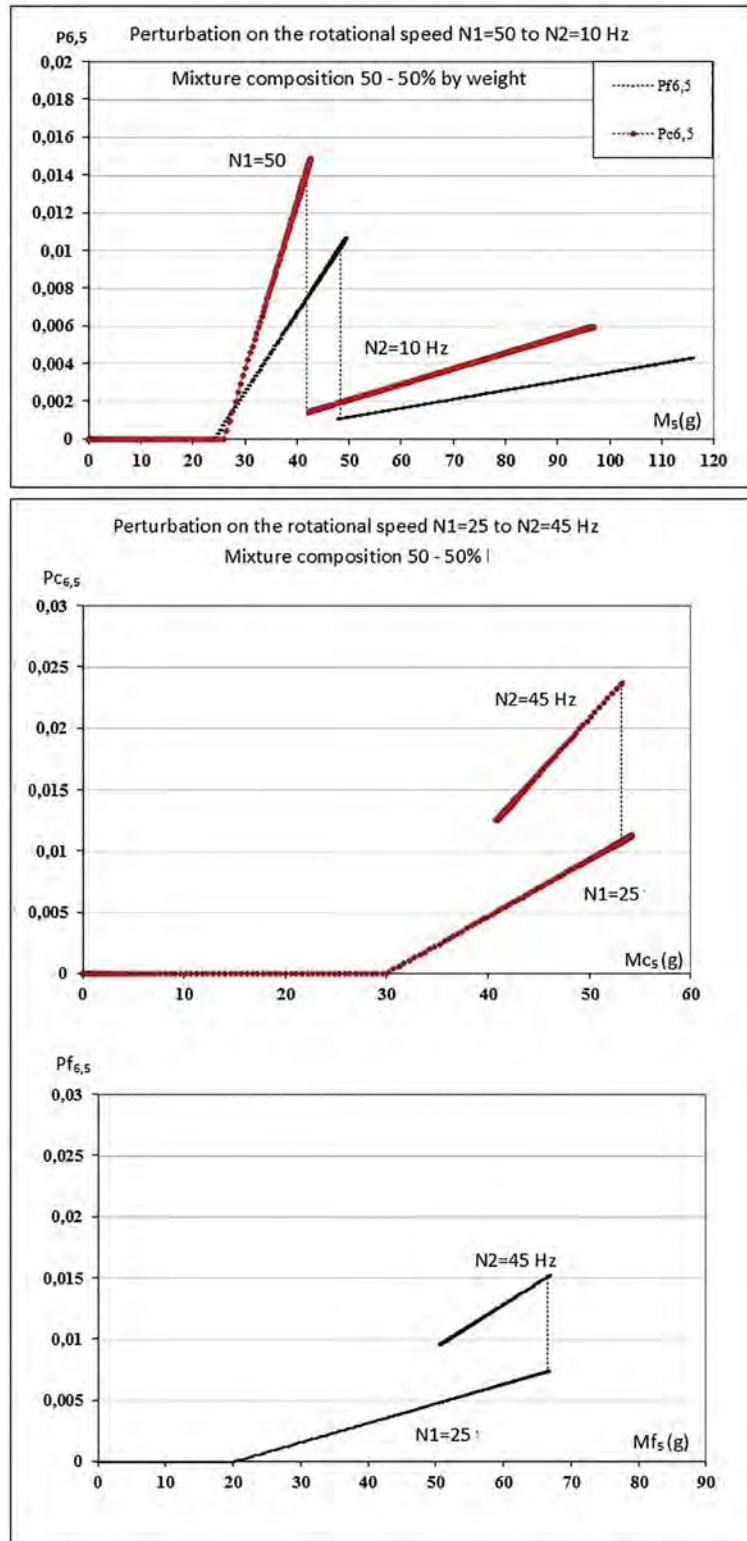
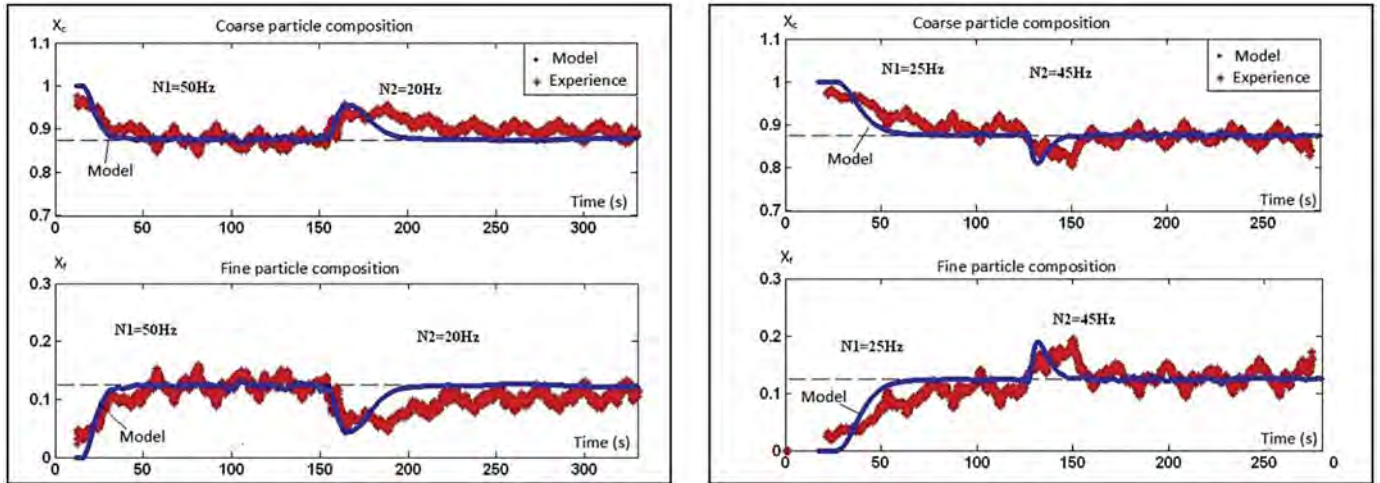
**B**

Fig. 21 (continued).

A negative step perturbation on the rotational speed (from 50 to 10 Hz) has been imposed to the system operating with mixture 1 and is depicted in Fig. 21a. In this graph, both coarse and fine products are represented. In the same figure, the results for a

positive step perturbation (from 25 Hz to 45 Hz) are shown. Whatever the case, the model is adequate in representing the evolution of the composition during the perturbation, in particular the way the system is able to reach another steady-state configuration.



**Fig. 22.** Simulation of negative and positive perturbation steps, mixture 2 - Comparison of the Markov chain model's results with the experiments in terms of outflow composition,  $Q_{in} = 40 \text{ kg h}^{-1}$ ,  $\Delta t = 0,1 \text{ s}$ .

The evolution of the transition probabilities during the whole process is presented in Fig. 21b, only for cell 5. In the case of the negative step, the probability increases with the local hold-up until it reaches the maximum value that corresponds to steady-state. At the time of the perturbation, this operating point is no longer valid. The system therefore has to catch the  $p_{65} - M_5$  line that corresponds to the operation under the new condition (10 Hz), afterwards the probability will evolve until it reaches the corresponding maximum value (approximately 0,006 for coarse particles). This is exactly the same that happens for the positive step (Fig. 21c), with the exception that at the moment of the perturbation, the probability that corresponds to the same hold-up – but for the higher stirrer's speed – is much higher (nearly 0,023) than the maximum probability under this operating condition (0,013). The path followed to reach this steady value is in fact the extension of the  $p_{65} - M_5$  line that can be drawn in a mixer start experiment under the condition  $N = 45 \text{ Hz}$ . Results relative to mixture 2 are presented in Fig. 22. They are globally similar to those obtained with mixture 1. However, it can be seen that the model fails in describing finely what happens during the two types of perturbation, in particular it predicts that the system will join steady-state earlier than in reality. Once again, the fluctuations that are appearing cannot be caught by the Markov chain in its present form. Various thoughts, underlining some of the model limitations, can be brought to partially explain this:

- The transition probabilities are defined for each component independently of the other, at the scale of the cells. Mixture 2, being mostly composed of coarse particles, could be more sensible to this hypothesis as the fine particles flow could be affected by the presence of the coarse particles. An improvement of the model would therefore be, for each component, to account for the presence of the other component in the transition matrix, for example by including a function of the composition directly in the probabilities.
- The time interval  $\Delta t$  chosen for the simulation is fixed and equal to 0.1 s. For a typical flow rate of  $40 \text{ kg h}^{-1}$ , this corresponds to 1 g, or roughly to 500 couscous particles. There is therefore a limitation to the use of equations (39) and (40) as they put together mass values that may correspond to 1000 times the particles involved in  $\Delta t$ .
- The mixture is dumped from the outlet mixer's gate onto the belt and conveyed through the image capture systems. There may be some segregation at the outlet gate or on the belt causing the variations in compositions that are experienced.

## 6. Concluding remarks

The Markov chain models developed in this work have proven their efficiency to catch the major process changes in terms of mass flows, mixture composition and hold-ups, for a wide range of typical process situations such as: mixer start, mixer stop, negative or positive steps on the rotational speed. They do not seem able to figure out the extent of the small-scale fluctuations on the composition of the mixtures that are recorded at the outlet of the equipment, especially for mixture 2 which is mainly composed of coarse particles by weight. It is unclear to what phenomena or factor this may be attributed.

Markov chains also need experimental input to calculate the transition probabilities, even if it can be done through various independent experiments. There is indeed a great interest, in process monitoring as well as in process development, in trying to link this input to the output of a DEM modelling scheme, so as to derive a hybrid model catching the whole system at any scale. Such models have emerged some ten years ago (see [17]) and are still looking very promising, although they need to be properly implemented to include the complexity of the particulate system and that of the mixer itself.

The intensification of the mixing process is also worth investigating. For instance, there is a lot of work to undertake in terms of stirrer design so as to induce perfect mixing in a horizontal configuration that is much proper to plug flow. The same holds true for the LIW feeders for which the smoothing of the mass flow fluctuations due to the feeding screw is a key issue. The location of these feeders along the mixer needs to be studied into details because, as we pointed out in the present work, segregation by percolation takes place close to the inlet wall. This means that it may be advisable to consider other feeding configurations, such as placing the segregating component's feeder to another place, and even so distributing the feed over the mixer's length. This has been theoretically considered by Mizonov et al. [31], again through a Markov chain model, but needs to be experimentally studied.

The immediate following step for this research work is to implement a process control loop, transforming the outlet mixture homogeneity signal into an action on the rotational stirrer's speed. This will help smoothing the fluctuations that appear during transitory phases or when LIW feeders are operating in the volumetric mode, like for hopper re-filling. This will be discussed in further papers.

## References

- [1] C. Ammarcha, C. Gatamel, J.L. Dirion, M. Cabassud, H. Berthiaux, Predicting the continuous powder mixing dynamics in transitory regimes, *Adv. Powder Technol.* 23 (2012) 787–800.

- [2] C. Ammarcha, C. Gatamel, J.L. Dirion, M. Cabassud, V. Mizonov, H. Berthiaux, Transitory powder flow dynamics during emptying of a continuous mixer, *Chem. Eng. Process. Process Intensif.* 65 (2013) 68–75.
- [3] C. Ammarcha, C. Gatamel, J.L. Dirion, M. Cabassud, H. Berthiaux, Continuous powder mixing of segregating mixtures under steady and unsteady state regimes: homogeneity assessment by real-time on-line image analysis, *Powder Technol.* 315 (2017) 39–52.
- [4] M. Aoun-Habbache, H. Berthiaux, M. Aoun, V. Mizonov, An experimental method and a Markov chain model to describe axial and radial mixing in a hoop mixer, *Powder Technol.* 128 (2–3) (2002) 159–167.
- [5] A. Auer, Das probabilistische modell des kontinuierlichen zerkleinern, *Powder Technol.* 28 (1981) 77–82.
- [6] I. Balagurov, V. Mizonov, H. Berthiaux, C.A. Gatamel, Markov chain model of mixing kinetics for ternary mixtures of dissimilar particulate solids, *Particuology* 31 (2017) 80–96.
- [7] H. Berthiaux, J.A. Dodds, Modeling classifier networks by Markov chains, *Powder Technol.* 105 (1–3) (1999) 266–273.
- [8] H. Berthiaux, Analysis of grinding processes by Markov chains, *Chem. Eng. Sci.* 55 (19) (2000) 4117–4127.
- [9] H. Berthiaux, V. Mizonov, Applications of Markov chains in particulate process engineering – a review, *Can. J. Chem. Eng.* 82 (2004) 1143–1168.
- [10] H. Berthiaux, K. Marikh, C. Gatamel, Continuous mixing of powder mixtures with pharmaceutical process constraints, *Chem. Eng. Process. Process Intensif.* 47 (2008) 2315–2322.
- [11] J. Bridgwater, Mixing of particles and powders: where next? *Particuology* 8 (2010) pp563–567.
- [12] M. Catak, N. Bas, K. Cronin, J.J. Fitzpatrick, E.P. Byrne, Discrete solution of the breakage equation using Markov chains, *Ind. Eng. Chem. Res.* 49 (2010) 8248–8257 17 pp.
- [13] M. Catak, N. Bas, K. Cronin, D. Tellez-Medina, E.P. Byrne, J.J. Fitzpatrick, Markov chain modelling of fluidised bed granulation, *Chem. Eng. J.* 164 (2010) 403–409.
- [14] W. Cho, S.W. Lee, J.H. Kim, Modeling and recognition of cursive words with hidden Markov models, *Pattern Recogn.* 28 (12) (1995) 1941–1953.
- [15] T.R.M. De Beer, C. Bodson, B. Dejaegher, P. Vercruysse, Burggraefe A. Raman spectroscopy as a process analytical technology (PAT) tool for the in-line monitoring and understanding of a powder blending process, *J. Pharm. Biomed. Anal.* 48 (2008) 772–779.
- [16] H.G. Dehling, A.C. Hoffman, H.W. Stuu, Stochastic models for transport in a fluidized bed, *SIAM J. Appl. Math.* 60 (1) (1999) 337–358.
- [17] J. Doucet, N. Hudon, F. Bertrand, J. Chaouki, Modeling of the mixing of monodisperse particles using a stationary DEM-based Markov process, *Comput. Chem. Eng.* 32-6 (2008) 1334–1341.
- [18] N. Ehrhardt, M. Montagne, H. Berthiaux, C. Gatamel, B. Dalloz-Dubrujeaud, Assessing the homogeneity of binary and ternary powder mixtures by on-line electrical capacitance, *Chem. Eng. Process.* 44 (2) (2005) 303–313.
- [19] L.T. Fan, Y. Chang, Mixing of large particles in two-dimensional gas fluidised beds, *Can. J. Chem. Eng.* 57 (1979) 88–97.
- [20] L.T. Fan, S.H. Shin, Stochastic diffusion model of non-ideal mixing in a horizontal drum mixer, *Chem. Eng. Sci.* 34 (1979) 811–820.
- [21] Y. Gao, F.J. Muzzio, M.G. Ierapetritou, Optimizing continuous powder mixing processes using periodic section modelling, *Chem. Eng. Sci.* 80 (2012) 70–80.
- [22] M. Ierapetritou, F. Muzzio, G. Reklaitis, Perspectives on the continuous manufacturing of powder-based pharmaceutical processes, *AIChE J.* 62 (6) (2016) 1846–1862.
- [23] V. Kehlenbeck, K. Sommer, A new model for continuous dynamic mixing of powders as well as in-line determination of the mixing quality by NIR spectroscopy, *World Congress on Particle Technology WCPT 4, 2002*, Sidney (Australia).
- [24] T.A. Kingston, T.J. Heindel, Granular mixing optimization and the influence of operating conditions in a double screw mixer, *Powder Technol.* 266 (2014) 144–155.
- [25] B.F.C. Laurent, J. Bridgwater, Performance of single and six-bladed powder mixers, *Chem. Eng. Sci.* 57 (2002) 1695–1709.
- [26] L. Legoix, C. Gatamel, M. Milhé, H. Berthiaux, Powder flow dynamics in a horizontal convective blender: tracer experiments, *Chem. Eng. Res. Des.* 121 (2017) 1–21.
- [27] K. Marikh, H. Berthiaux, V. Mizonov, E. Barantseva, Experimental study of the stirring conditions taking place in a pilot plant continuous mixer of particulate solids, *Powder Technol.* 157 (2005) 138–143.
- [28] K. Marikh, H. Berthiaux, V. Mizonov, E. Barantseva, D. Ponomarev, Flow analysis and Markov chain modelling to quantify the agitation effect in a continuous powder mixer, *Chem. Eng. Res. Des.* 84-A11 (2006) 1059–1074 *Trans IChemE Part A*.
- [29] K. Marikh, H. Berthiaux, C. Gatamel, V. Mizonov, E. Barantseva, Influence of stirrer type on mixture homogeneity in continuous powder mixing: a model case and a pharmaceutical case, *Chem. Eng. Res. Des.* 86 (2008) 1027–1037.
- [30] I. Martinez, A. Peinado, L. Liesum, G. Betz, Use of near-infrared spectroscopy to quantify drug content on a continuous blending process: influence of mass flow and rotation speed variations, *Eur. J. Pharm. Biopharm.* 84 (3) (2013) 606–615.
- [31] V. Mizonov, H. Berthiaux, C. Gatamel, Theoretical study of optimal positioning of segregating components input into continuous mixer of solids, *Part. Sci. Technol.* 33 (4) (2015) 339–341.
- [32] R. Nassar, S.T. Chou, L.T. Fan, Modelling and simulation of deep-bed filtration, a stochastic compartmental model, *Chem. Eng. Sci.* 41 (1986) 2017–2027.
- [33] J. Osorio, F.J. Muzzio, Effect of processing parameters and blade patterns on continuous pharmaceutical powder mixing, *Chem. Eng. Process. Process Intensif.* 109 (2016) 59–67.
- [34] L. Pernenkil, C.L. Cooney, A review on the continuous blending of powders, *Chem. Eng. Sci.* 61 (2006) 720–742.
- [35] P.E. Pfeifer, R.L. Carraway, Modeling customer relationships as Markov chains, *J. Interact. Mark.* 14 (2) (2000) 43–55.
- [36] K. Plumb, Continuous processing in the pharmaceutical industry: changing the mindset, *Chem. Eng. Res. Des.* 83 (2005) 730–738.
- [37] D. Ponomarev, V. Mizonov, H. Berthiaux, J. Gyenis, C. Gatamel, E. Barantseva, A 2-D Markov chain for modelling powder mixing in alternately revolving static mixers of Sysmix® type, *Chem. Eng. Process. Process Intensif.* 48 (2009) 1495–1505.
- [38] P. Portillo, P.G. Ierapetritou, F.J. Muzzio, Characterization of continuous convective powder mixing processes, *Powder Technol.* 182 (2008) 368–378.
- [39] R. Ramachandran, J. Arjunan, A. Chadhury, M.G. Ierapetritou, Model-based control-loop performance of a continuous direct compaction process, *J. Pharm. Innov.* 6 (2011) 249–263.
- [40] F. Roche, T. Page, J. Seville, Non-stop Pharma: Centuries in the Making, *The Chemical Engineer*, February 2013 28–31.
- [41] A.D. Sahin, Z. Sen, First-order Markov chain approach to wind speed modelling, *J. Wind Eng. Ind. Aerodyn.* 89 (3–4) (2001) 263–269.
- [42] A. Sarkar, C.R. Wassgren, Simulation of a continuous granular mixer: effect of operating conditions on flow and mixing, *Chem. Eng. Sci.* 64 (2009) 2672–2682.
- [43] M. Sen, R. Singh, A. Vanarase, J. John, R. Ramachandran, Multi-dimensional population balance modelling and experimental validation of continuous powder mixing processes, *Chem. Eng. Sci.* 80 (2012) 349–360.
- [44] M. Sen, R. Ramachandran, A multi-dimensional population balance model approach to continuous powder mixing processes, *Adv. Powder Technol.* 24 (2013) 51–59.
- [45] R. Singh, F.J. Muzzio, M. Ierapetritou, R. Ramachandran, A combined feed-forward/feed-back control system for a QbD based continuous tablet manufacturing process, *PRO 3* (2015) 339–356.
- [46] A. Tamir, Applications of Markov Chains in Chemical Engineering, Elsevier ed, Amsterdam, 1998.
- [47] J.D. Tjakra, J. Bao, N. Hudon, R. Yang, Collective dynamics modeling of polydisperse particulate systems via Markov chains, *Chem. Eng. Res. Des.* 91 (2013) 1646–1659.
- [48] E.M. Tory, D.K. Pickard, A three-parameter Markov model for sedimentation, *Can. J. Chem. Eng.* 55 (1977) 655–665.
- [49] A.U. Vanarase, F.J. Muzzio, Effect of operating conditions and design parameters in a continuous powder mixer, *Powder Technol.* 208 (2011) 26–36.
- [50] R.H. Wang, L.T. Fan, Axial mixing of grains in a motionless Sulzer (Koch) mixer, *Ind. Eng. Chem. Process. Des. Dev.* 15 (3) (1976) 381–388.
- [51] R. Weinekötter, L. Reh, Continuous mixing of fine particles, *Part. Part. Syst. Charact.* 12 (1995) 46–53 1 pp.
- [52] J. Wei, W. Lee, F.J. Krambeck, Catalyst attrition and deactivation in FCC system, *Chem. Eng. Sci.* 32 (1977) 1211–1218.
- [53] Z. Wu, O. Tao, X. Dai, M. Du, X. Shi, Y. Qiao, Monitoring a pharmaceutical blending process using near-infrared chemical imaging, *Vibration. Spectros.* 63 (2012) 371–379.
- [54] X. Zhao, C. Gatamel, J.L. Dirion, H. Berthiaux, M. Cabassud, Implementation of a control loop for a continuous powder mixing process, *AIChE annual meeting*, San Francisco (CA), 2013, November.
- [55] Y. Zhuang, X. Chen, D. Liu, Stochastic bubble developing model combined with Markov process of particles for bubbling fluidized beds, *Chem. Eng. J.* 291 (2016) 206–214.